Status of Novosibirsk Free Electron Lasers and Their Applications to Study of Fast Processes

G. Kulipanov[1], E. Chesnokov[2], Ya. Getmanov[1], V. Kubarev[1], O. Shevchenko[1], A. Vasiliev[3], N. Vinokurov[1].

[1]*Budker Institute of Nuclear Physics, 630090 Novosibirsk, Russia*
[2]*Institute of Chemical Kinetic and Combustions, 630090 Novosibirsk, Russia.*
[3]*Lavrentyev Institute of Hydrodynamics, 630090 Novosibirsk, Russia.*
kulipanov@inp.nsk.su

Abstract: A description and parameters of free electron lasers, based of the four-track energy recovery linac, are given. The results on investigations of rapid processes are presented. The prospects of further work are discussed.

The Novosibirsk FEL facility is based on the four-turn energy recovery linac (ERL). The ERL can operate in three modes, providing electron beam for three different FELs. The whole facility can be treated as three different ERLs (one-turn, two-turn and fourturn), which use the same injector and the same linac [1].

Parameters of the laser radiation for the three laser systems of NovoFEL are presented in Table 1, where λ is wavelength; $\delta\lambda/\lambda$ is the relative linewidth; (P) is the maximum average power; P_{peak} is the maximum peak power; τ is the pulse length; f_{opt} is the round-trip optical cavity frequency. The radiation is linearly polarized.

Table 1. Radiation parameters of NovoFEL lasers.

	1st FEL	2nd FEL	3rd FEL
In operation from	2003	2009	2015
Wavelength, μm	90 - 240	40 - 90	5 - 40
Line width, %	0.3 – 1.0	0.2 - 1.0	0.1 – 1.0
Average power, kW	0.5	0.5 – 1.0	10
Peak power, MW	1.0	2.0	10
Pulse duration, ps	40 - 100	20 - 40	10 - 20

The NovoFEL radiation is extracted from the optical cavity through an opening of 8 mm in diameter in the tail-end mirror and enters into the beamline passing an 1 mm thick diamond output window. Drayed air-nitrogen mixture is continuously circulated inside the beamline to avoid absorption of terahertz radiaton by water vapor.

Six user stations (chemistry station, metrology station, molecular spectroscopy station, biology station, vacuum station, station for spectroscopy and imaging) and two diagnostic stations are in operation now. Another four are under construction. A small fraction of radiation is split to a spectrometer, which allows continuous measurement of the radiation spectrum while users are performing their experiments. Other radiation diagnostics include a Fourier spectrometer, a thermograph, microbolometer arrays, a pyroelectric array, and a fast Schottky diode coupled to a 20 GHz oscilloscope. The last one is used for time-resolved measurements.It allows recording the laser pulse shape and other signals with time resolution up to 15 ps [2].

Optical elements for manipulation and shaping of laser radiation, as well as for experiments on terahertz imaging, were designed and fabricated. A limited number of substances are suitable for use as “optical quality” transparent materials in the terahertz range. High-numerical-aperture kinoform lenses made of high-density polypropylene 0.8 mm thick, which turned out to be resistant to intense THz radiation, enabled obtaining images with a diffraction-limited resolution. Another radiation-resistant material, high-resistivity silicon, has better mechanical characteristics and many technological processes can be applied to its treatment. These capabilities were used in the creation of a set of binary diffraction optical elements (DOEs).

Imaging Devices. Uncooled 160 120 and 320x240 microbolometer arrays (MBA) with a pixel size of 51x51 μm and a repetition rate of up to 90 frames per second have been adapted to the terahertz imaging. The sensitivity of an array with a germanium window to terahertz radiation at λ = μm was found to be 30 nW/pixel, which proves the array to be a rather sensitive imager with an excellent wavelength-limited spatial resolution [3].

One-Channel Radiation Detectors. The user stations are equipped with a large collection of one-channel THz radiation detectors. Besides the above mentioned fast Schottky diodes, pyroelectric and bolometer detectors are used.

Selected experiments. Quasi-Continuous Terahertz Optical Discharge [4]. Nonlinear interaction of the high-power terahertz radiation of the Novosibirsk FEL with matter demonstrates an interesting phenomenon of terahertz optical discharge. It was attained immediately after commissioning of the Novosibirsk FEL and spectacularly demonstrated the high pulse power of the latter. Currently, experiments with such discharge are systematically carried out at the Novosibirsk FEL. They are of both metrology character (measurement of the discharge occurrence and maintenance thresholds for different gases and substances) and research nature (search for useful applications of this type of discharge). With short pulses of the Novosibirsk FEL (70 ps), a terahertz optical discharge occurs with pulsed fields of focused radiation of ~1 MV/cm and pulse intensities of ~ 1 GW/cm^2 and, unlike other terahertz laser sources, the discharge can be quasi-continuous. The discharge dynamics is complex and diverse. In particular, gas dynamic auto-oscillations and plasma oscillations arise in it at nonlinear frequencies.

Ultra-fast high-resolution spectroscopy [5] is an important field of research at the Novosibirsk terahertz free electron laser (NovoFEL). It uses almost all the advantages of the NovoFEL radiation (wavelength tuning, high pulsed power, and continuous pulse train). This spectroscopy is based on the measurement of signals of free-induction decay (FID) of emission by molecules excited with short (70–100 ps) NovoFEL pulses. Such signals are measured via slow step-by-step scanning in all time-domain spectrometers. The high pulse power of NovoFEL enabled first real-time measurement of terahertz signals with specially developed ultrafast detectors. This allows ultrafast single-pulse terahertz spectroscopy, which is the only possible in study of single and non-recurring processes, creation of spectrographic "movies" on the basis of the NovoFEL pulse-periodic radiation etc. Our subsequent measurements showed that FID signals can be up to 180 ns long, which enables a spectral resolution of about 6 MHz (3 10^{-6}) .

Investigating nonstationary waves from the combustion and detonation of a hydrogen–oxygen mixture in the optical and Terahertz Ranges [6]. A combustion wave initiated in a cylindrical channel 40 mm in diameter and 1 m in length with a dried mixture of $2H_2 + O_2$ during investigations using the absorption line of water at 130 μm had a complex structure. The characteristic stages of the process, measured at a distance of 300 mm from the point of ignition, occurred in the time interval of 2 ms to 30 ms and corresponded to velocities of 10–160 m s^{-1}. These velocities are typical of laminar and accelerating turbulent subsonic combustion.

The investigation was conducted in different parts of the cylindrical channel at distances $L1$ = 300 mm and $L2$ = 700 mm from the place of ignition. Investigations were conducted using the radiation at the OH radical absorption line 119.3 μm (83.8 cm–1) and after tuning away from the line. Correlation between the absorption of terahertz radiation, the optical signal, and the acceleration of the flame front with the formation of a bow shock wave was observed at times on the order of several milliseconds. Absorption was on the order of 20% on the OH radical line at a distance of 300 mm from the point of ignition at the moment of the light signal's maximum brightness. The absorption maximum was observed 13–14 ms after ignition and was as high as 80%. The form of signals on the absorption lines and upon tuning away from them showed that along with the useful signal apparently produced in the later stages of absorption (after tens of milliseconds), there were spurious absorption signals from refraction on plasma and Rayleigh scattering on water drops. The data obtained in this work on the substantial absorption of terahertz radiation by the reaction products from the combustion of a hydrogen–oxygen mixture (H_2O and OH) could serve as the basis for developing a more advanced device consisting of several simultaneously operating Schottky detectors, spaced along the axis of a cylindrical channel, with reduced sensitivity to the refraction deviation of terahertz radiation. A line (strip) of fast Schottky detectors is also needed to observe the dynamics of a front's complex structure. As of now, there is no such strip, and one must be developed.

[1] Kulipanov G.N., Bagryanskaya E.G., Chesnokov N.A., et al. Novosibirsk free electron laser – facility description and recent experiments // IEEE transactions on terahertz science and technology. – 2015. – Vol. 5, No 5. – P. 798-809.

[2] Knyazev B.A., Kulipanov G.N., Vinokurov N.A. Novosibirsk terahertz free electron laser: instrumentation development and experimental achievements // Measurement science and technology. – 2010. – Vol. 21. – P. 054017 (13 p.)

[3] Dem'yanenko M.A., Esaev D.G., Knyazev B.A., Kulipanov G.N., Vinokurov N.A. Imaging with a 90 frames/s microbolometer focal plane array and high-power terahertz free electron laser // Applied physics letters. – 2008. – Vol.92., No 13. - P. 131116-1 – 131116-3.

[4] Kubarev V.V. Dynamics of the THz optical discharge // Proceedings of Joint 39th International conference on infrared, millimeter, and terahertz waves, IRMMW-THz 2014, Tucson, Arizona, USA, 14-19 Sept. 2014. – S/l/, 2014. – P. 6956280. – T_A-162_Kubarev.pdf. – DOI 10.1109/IRMMW-THz.2014.6956280.

[5] Chesnokov E.N., Kubarev V.V., Koshlyakov P.V., Kulipanov G.N. Very long terahertz free induction decay in gaseous hydrogen bromide // Laser physics letters. – 2013. Vol. 10, No 5. –P. 055701 [3 p.].

[6] Vasiliev A.A., Palchikov E.I., Kubarev V.V., Chesnokov E.N., Koshlyakov P.V., Dolgikh A.V., Krasnikov I.Yu. Investigating nonstationary waves from the combustion and detonation of a hydrogen-oxygen mixture in the optical and terahertz ranges // Bulletin of the Russian Academy of Sciences. Physics. – 2015. – Vol. 79, N0 9. –P. 1202-1207.

ULTRA Laser Facility Applications for Chemistry, Life Sciences and Catalysis

Igor V. Sazanovich[1], Gregory M. Greetham[1], Ian P. Clark[1], Inés Lezcano-González[2,3], Andrew M. Beale[2,3], Milan Delor[4], Julia A. Weinstein[4], James P. Hall[5,6], Susan J. Quinn[7], Pavel Matousek[1], Anthony W. Parker[1], Michael Towrie[1]

[1]Central Laser Facility, STFC, Research Complex at Harwell, Rutherford Appleton Laboratory, Oxfordshire, OX11 0QX, UK. [2]Research Complex at Harwell, Rutherford Appleton Laboratory, Oxfordshire, OX11 0FA, UK. [3]Chemistry Department, University College London, Gordon Street, London, WC1H 0AJ, UK. [4]Department of Chemistry, University of Sheffield, Sheffield, S3 7HF, UK. [5]Department of Chemistry, University of Reading, Whiteknights, Reading RG6 6AD, UK. [6]Diamond Light Source, Harwell Campus, Oxfordshire, OX11 0QX, UK. [7]School of Chemistry, University College Dublin, Dublin 4, Ireland

Abstract: We describe ULTRA laser facility applications for chemistry, life sciences and catalysis, illustrated by vibrational control of electron transfer; photoinduced electron transfer in DNA crystals; and *operando* Kerr-gated Raman insight into catalytic hydrocarbon conversion with zeolites.

1. Introduction

The Central Laser Facility ULTRA facility is based at the Rutherford Appleton Laboratory (Oxfordshire, UK) in a unique multidisciplinary environment. The ULTRA facility is a state-of-the-art instrument designed to perform diverse ultrafast time-resolved laser spectroscopy experiments in the broad spectral range from UV to mid-IR [1,2]. Here we describe how we employed ULTRA to achieve vibrational control of light-induced charge transfer in donor–bridge–acceptor assemblies, and to define both the geometry of the reaction site and the rates of individual steps in a reversible photoinduced electron-transfer between ruthenium polypyridyl and DNA in the crystal environment. We also demonstrate how we shed a new light on the problem of zeolite deactivation by operando Kerr gated Raman monitoring of a catalytic reaction.

2. Vibrational control of electron transfer

Photoinduced electron transfer (ET) is a fundamental process enabling some of Nature's most important reactions, e.g. photosynthesis, and is instrumental for photovoltaics operation. Therefore it is highly desirable to develop the means to steer electron transfer to alter the outcome of the reaction and the overall yield.

In this work we demonstrate how we can steer the electron transfer with low-energy infrared photons by selective mid-IR excitation of the bridge in a range of Acceptor-Donor transition metal complexes linked by a acetylide bridge [3,4]. The systems studied and the schematics of the experiment are shown in Fig. 1. To initiate the electron transfer we excited the systems with the 50 fs laser pulse at 400 nm, and then a few picoseconds later, while the system is still "at the crossroads" in the non-equilibrium vibronic state, we perturb the system with narrow-band 2 ps mid-IR pulse at ca. 1900 cm^{-1}.

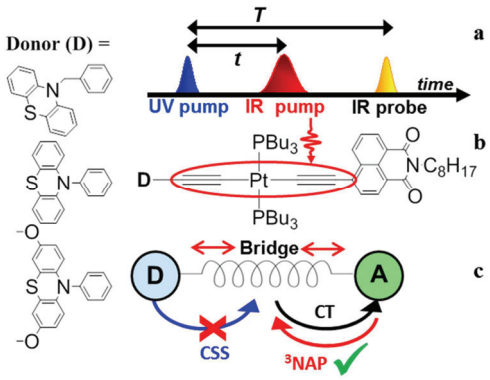

Fig. 1. The structure of the Donor-Acceptor systems studied (left and middle), the pulse sequence used in the experiments (top right), and the effect on the excited state.

We managed to suppress the formation of the distant charge-separated state; the size of the effect depends on the donor type used (Fig. 1) and can reach 100%. The excited molecules are re-directed instead towards populating intra-ligand triplet state and re-forming the ground state.

3. One-electron guanine photo-oxidation in DNA crystals

Photoinduced DNA damage is an important reaction leading to light-induced diseases (including skin cancer) but also instrumental for photodynamic therapy of cancer when photosensitiser drugs are used. The majority of the studies in this area have been done in solution, however in solution phase it is very difficult to define the precise location and orientation of the photosensitiser vs. DNA bases. Furthermore, it is impossible to achieve in solution phase the high drug concentration and molecularly crowded environment that drugs encounter in the cell.

To address those questions we performed the first ever ultrafast time-resolved laser spectroscopy study of photosensitised DNA oxidation in the crystal phase. We used ruthenium polypyridyl photosensitiser Λ-$[Ru(TAP)2(dppz)]^{2+}$ bound to $(TCGGCGCCGA)_2$ sequence of nucleic bases (Fig. 2), for which the structure and orientation of all counterparts in the crystal samples have been precisely established [5]. To overcome the strong scattering due to the micro crystals (up to 5 μm is size) the experiments were performed in the mid-IR while exciting samples at 400 nm.

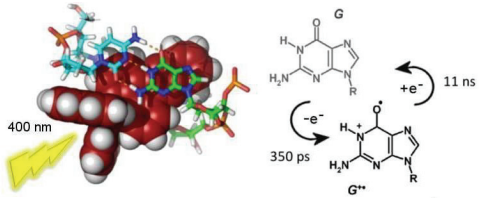

Fig. 2. The diagram of the ruthenium polypyridyl complex binding to the DNA sequence, and the forward/reverse electron transfer to guanine.

In the transient infrared data we observed formation of guanine radical cation evidenced by 1709 cm^{-1} band which decays concomitantly with the decay of the excited state signal (major feature at 1456 cm^{-1}) and ground state recovery (1275 cm^{-1} band) of Λ-$[Ru(TAP)2(dppz)]^{2+}$. The experiments revealed the individual steps in the photoinduced reversible electron transfer reaction in DNA crystals, indicating that the dynamics observed in the crystal state are similar to those in solution [6].

4. *Operando* Kerr-gated Raman monitoring of hydrocarbon conversion on zeolites

Zeolites are widely used as catalysts in the chemical industry for large-scale hydrocarbon conversion processes such as catalytic cracking, reforming or methanol-to-hydrocarbons. A major issue with these technologies is the progressive deactivation of the catalyst by the formation of carbon deposits, leading to a decline in process efficiency. To optimise catalyst performance, it is then required to understand the structure, formation mechanism and deactivating role of carbon deposits [7].

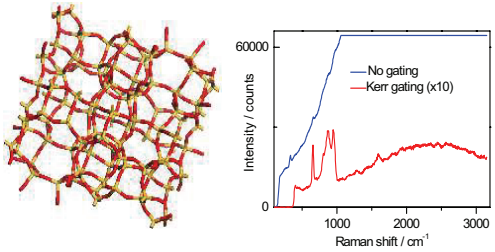

Fig. 3. ZSM-5 zeolite structure (left) and illustration of the power of Kerr gating to detect the Raman signal of Mo-ZSM-5 zeolite (right).

Raman spectroscopy is a powerful technique for characterising carbon species. However, its application to zeolite catalysts is often limited by strong sample fluorescence that dominates the Raman signal. In this work, we have followed the catalysis with Raman spectroscopy using ULTRA as a bright visible excitation source in combination with a Kerr-gated spectrometer to 'circumvent' fluorescence, in order to examine the evolution of carbon species in two relevant zeolite-based processes, i.e. methane dehydroaromatisation (MDA) and methanol-to-hydrocarbons (MTH). The results obtained have allowed us to identify the formation of graphitic carbon (Raman signatures at 1390 cm^{-1} and 1610 cm^{-1}) after the MDA reaction, as well as catalytically important carbon-containing species (aromatic/aliphatic) during the course of the MTH.

5. References

[1] G.M. Greetham, et. al., "ULTRA: A Unique Instrument for Time-Resolved Spectroscopy," Appl. Spectrosc., **64**, 1311-1319 (2010).

[2] G.M. Greetham, et. al., "A 100 kHz Time-Resolved Multiple-Probe Femtosecond to Second Infrared Absorption Spectrometer," Appl. Spectrosc., **70**, 645-653 (2016).

[3] M. Delor, et. al., "Toward control of electron transfer in donor-acceptor molecules by bond-specific infrared excitation," Science, **346**, 1492-1495 (2014).

[4] M. Delor, et. al., "On the mechanism of vibrational control of light-induced charge transfer in donor–bridge–acceptor assemblies," Nature Chem., **7**, 689-695 (2015).

[5] J. P. Hall, et al., "Structure determination of an intercalating ruthenium dipyridophenazine complex which kinks DNA by semiintercalation of a tetraazaphenanthrene ligand," Proc. Natl Acad. Sci. USA, **108**, 17610–17614 (2011).

[6] J.P. Hall, et. al., "Monitoring one-electron photo-oxidation of guanine in DNA crystals using ultrafast infrared spectroscopy," Nature Chem., **7**, 961-967 (2015).

[7] M. Guisnet, et al. "Prevention of zeolite deactivation by coking," J. Molec. Catal. A, **305**, 69-83 (2009).

High-Voltage Pico- and Nanosecond Discharge Development in Gaseous and Liquid Media

N.L. Aleksandrov
Moscow Institute of Physics and Technology, Dolgoprudny, Moscow region, 141700 Russia
nick_aleksandrov@mail.ru
E.M. Anokhin
Moscow Institute of Physics and Technology, Dolgoprudny, Moscow region, 141700 Russia
eu.anokhin@gmail.com
I.N. Kosarev
Moscow Institute of Physics and Technology, Dolgoprudny, Moscow region, 141700 Russia
ilyakosarev@gmail.com
A.Yu. Starikovskiy
Princeton University, Princeton, NJ08544, USA
astariko@princeton.edu

Abstract: Fast imaging study of high-voltage pulsed discharges in a wide density range is reviewed. Focus is on fast ionization waves, streamer and dielectric barrier discharges in gases and on pulsed discharges in liquids.

1. Introduction

Generation of chemically active excited molecules, atoms and radicals is important for some applications of nonequilibrium discharge plasmas. These active species are efficiently generated in electron-molecule collisions for sufficiently high electron energies. In weakly-ionized discharge plasmas, the average electron energy and the rates of high-energy electron collisions are controlled by the reduced electric field E/N, where N is the gas number density. High-voltage pulsed discharges are attractive for applied purposes because they permit the generation of nonequilibrium plasmas for high values of E/N, much higher than the breakdown threshold. The properties of these discharges vary drastically with the density of media in which they are initiated.

The aim of this paper is, using fast imaging study, to show how the properties and dynamics of high-voltage pulsed discharges change with increasing density of the medium in which the discharges develop, from low-pressure gases to liquids.

2. Fast ionization waves

High-voltage nanosecond discharges develop within long dielectric tubes in the form of a fast ionization wave propagating with a velocity of $10^9 – 10^{10}$ cm/s. The wave propagates from the high-voltage electrode to the low-voltage one. High electric fields in the ionization wave and behind it lead to efficient generation of atoms, radicals, electronically excited neutral particles and ionized species in electron collisions with molecules. Fast imaging of the discharge gap showed that the plasma produced in gases at pressures of around several tens of Torr and room gas temperature is uniform when the high-voltage pulse amplitude is in the range 5 – 15 kV [1]. An increase in the voltage amplitude caused an increase in gas pressures for which spatially uniform plasma was generated by the fast ionization wave. The uniformity of the discharge plasma is associated with the generation of high-energy electrons that move ahead of the ionization front and provide uniform pre-ionization of the gas.

Fast ionization waves in long dielectric tubes also have been studied at high (up to 1 atm) gas pressures in connection with the problem of gaseous detonation initiation in pulsed detonation engines. Fast imaging study at high overvoltages showed several stages of gas discharge development for high pressures. Firstly, a fast ionization wave propagated from the high-voltage electrode to the ground electrode. Then, after bridging the discharge gap, a return wave was initiated near the ground electrode and propagated in the opposite direction.

Plasma generation by a fast ionization wave has been studied with fast imaging in chemically active preheated combustible gaseous mixtures to address the problem of plasma-assisted ignition. For this purpose, a high-voltage nanosecond discharge was initiated in gaseous combustible mixtures heated up to 1000 – 2000 K behind the reflected shock wave in a shock tube with a discharge chamber. Ignition delay time was measured, using emission spectroscopy methods, with the discharge and without it. It was shown that the discharge initiation leads to orders of magnitude reduction in the ignition delay time for various gaseous fuels. According to fast imaging at the discharge and ignition stages, generation of uniform plasma caused uniform ignition of combustible mixtures at pressures of ~ 1 atm [2]. This made it much easier to theoretically simulate generation of chemically active species during the discharge phase and chemical kinetics during ignition.

3. Streamer discharges

In open gases, high voltage discharges usually develop in the form of streamer (filamentary) discharges that have numerous applications including breaking electrical insulation, gas cleaning and ozone production. ICCD images

of the discharge gap were used to study the discharge structure that is usually branched. It was shown that the number of branches increases with pressure at fixed applied voltage and increases with voltage at fixed pressure. Solitary streamer channels were observed only at low pressures, below 470 Torr in air at a voltage of 24 kV in the point-to-plane geometry with a discharge gap of 3 cm.

Bridging the gap by a streamer channel can be followed by the formation of an arc (electrical breakdown). Streamer breakdown occurs even in under-critical electric fields when the discharge is in a repetitively pulsed regime. In this case, from fast imaging, the first discharge in the burst began with the formation of a small ionized region in the vicinity of the tip of the high-voltage electrode. The expansion of the ionized region led to a sharp decrease in the electric field on its boundary. The channel elongated towards the opposite electrode and came to rest when the applied voltage collapsed. The next voltage pulse in the burst produced the discharge in the gap with non-uniform gas density (due gas heating) and ionization. The discharge developing in the pre-heated and pre-ionized gas bridged the gap and formed an arc.

4. Dielectric barrier discharges

A surface dielectric barrier discharge is characterized by extremely high electric fields and is promising for plasma aerodynamics, plasma-assisted ignition and some other applications. This discharge usually starts from the high-voltage electrode and develops along the surface of a dielectric layer located between the high-voltage and grounded electrodes. Fast imaging showed that the pulse discharge flashes are observed twice per one pulse, one on the leading voltage pulse edge and another on the trailing pulse edge [3]. The discharge plasma manifested itself as a number of thin filaments (streamers) propagating along the dielectric surface. Emission was observed from the whole streamer channels, as opposed to streamers in open gases when emission is usually radiated only from the leading ionization front. The dielectric surface was charged during streamer propagation. Therefore, when the trailing edge of the high-voltage pulse reached the electrode, its potential became smaller than the potential of the dielectric surface in the discharge gap. This led to the initiation of the second flash that corresponded to the charge removal from the surface.

5. Pulsed discharges in liquids

Discharge processes in liquids have been of interest for a long time, beginning with the analysis of electrical insulation properties in various systems. Recently, the range of possible applications for discharges in liquids was extended to water sterilization, biomedical applications and water quality control. New applications require liquid excitation with a minimal temperature increase. The simplest solution to the problem is to shorten applied high-voltage pulses.

Observations with various voltage pulse duration, using different techniques including fast imaging, showed that there are three possible mechanisms for discharge propagation in liquid, depending on the pulse duration [4]. When a microsecond pulse is applied to the electrodes in non-conducting liquid, discharge develops in low density regions (bubbles). These low density regions can be pre-existing due to dissolved gases or can be generated by local heating (energy injection from the electrode by pre-breakdown currents) and cavitation. Under nanosecond pulse conditions, in the ionization wave front, an extreme electric field provides a strong negative pressure by electrostriction forces in the liquid to form initial micro-voids in the continuous medium. In these voids, electrons efficiently gain energy in the electric field and provide starting points for plasma generation. In the case of picosecond pulses, reduced density regions have no time to be formed because of the extremely short pulse duration. Ionization in liquid occurs due to direct electron impact without any phase transition; electrons are accelerated in an external electric field that is comparable with atomic fields. Here, the discharge develops with a velocity comparable to the local light speed. The effect of liquid permittivity is important for the discharges under nanosecond pulses and is small for microsecond and picosecond pulses.

6. Conclusions

Fast imaging technique provides a unique way to study high-voltage pulsed discharges in various media, from low-pressure gases to liquids. The degree of plasma uniformity and sequence of different stages of the discharge plasma evolution are easy to reproduce with ICCD images on nanosecond and picosecond scales.

[1] N. B. Anikin, N. A. Zavialova, S. M. Starikovskaia and A. Yu. Starikovskii, “Nanosecond discharge development in long tubes”, IEEE Trans. Plasma Sci. **36**, 902-903 (2008).

[2] S. M. Starikovskaia, E. N. Kukaev, A. Y. Kuksin, M. M. Nudnova and A. Yu. Starikovskii, “Combustion initiated by nonequilibrium plasma”, IEEE Trans. Plasma Sci. **36**, 1312-1313 (2008).

[3] D. V. Roupassov and A. Yu. Starikovskii, “Development of nanosecond surface discharge in actuator geometry”, IEEE Trans. Plasma Sci. **36**, 904-905 (2008).

[4] A. Starikovskiy, Y. Yang, Y. Cho and A. Fridman, “Nonequilibrium plasma in liquid water: Dynamics of generation and quenching” Plasma Sources: Sci. Technol. **20**, 024003 (2011).

Study of Single Femtosecond Filamentation in Gas by Transverse Interferometry Method

P.A. Chizhov, V.V. Bukin, A.A. Ushakov, S.V. Garnov

Prokhorov General Physics Institute of Russian Academy of Sciences, Moscow, Russia, Vavilov. str., 38

pvch@inbox.ru

Abstract: Anisotropy of refractive index due to intense laser pulse propagation is observed. Nonlinear dependence of initial electron density in air and nitrogen on pressure is stated. Plasma decay is observed via hundreds of picoseconds.

1. Introduction

Filamentation of femtosecond laser radiation attracts scientific attention for more than two decades as this process is accompanied by many other nonlinear effects due to high intensity in the core of the filament. These are, for example, generation of X-ray, UV high harmonics, supercontinuum and terahertz radiation[1,2]. Several methods exist to measure spatial properties of the filament plasma channel and the plasma density inside based on conductivity measurement[3], fluorescence measurement[4], pump-probe techniques including transverse interferometry[5-7]. Some of them need calibration by other methods, which allow to measure electron density directly. Transverse interferometry technique is one of these direct measurement methods.

Our goal was to investigate the process of formation of the filament plasma channel and to observe the decay of plasma in gases under different pressure during the first hundreds picoseconds using this method.

2. Experiment and data processing

Ti:Sa-laser beam was split in two parts. Powerful one created filament in the gas chamber by focusing with 500 mm focal length lens. The other beam was used as a probe beam passing through a plasma channel area and then creating interferometric pattern on digital camera. Two series of interferogramms were obtained: with probe beam passing through plasma channel (signal, pump beam open) and unionized gas (background, pump beam closed). After that these interferogramm series were processed by Fourier filtration technique to obtain mean phase shift due to plasma presence[8,9]. Refractive index change profile and corresponding plasma density profile were calculated by inverse Abel transformation of phase shift profiles.

3. Results

We observed the decay of plasma under atmospheric pressure in air, nitrogen and argon for two durations of the laser pulse: 40 fs and 150 fs. Initial peak plasma density in case of 150 fs pulse is about 70 % of that for 40 fs pulse(Figure 1).

In case of 150 fs pulse filamentation in air a nonlinear dependence of initial plasma channel peak electron density is observed(Figure 2(a)), it is stated that this increase is accompanied by plasma channel diameter decrease (Figure 2(b)). Plasma density rises almost 2 times between 3 and 4 atm.

Optical refractive index anisotropy, which precedes and accompanies ionization, related with intense pulse propagation is revealed(Figure 3(b)).

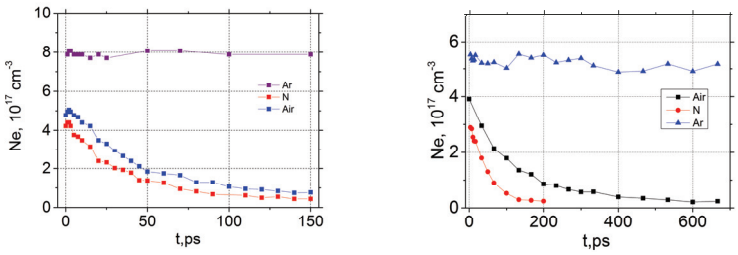

(a) (b)

Figure 1. Electron density dependence on time after ionization: (a) for 40 fs pulse; (b) for 150 fs pulse.

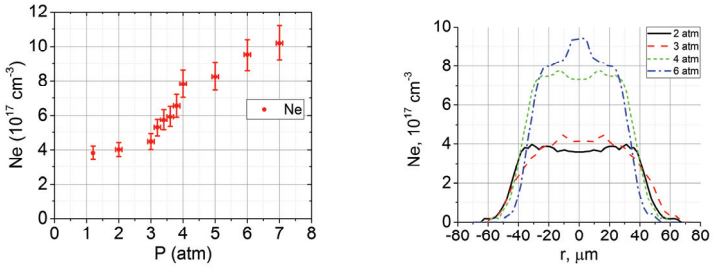

(a) (b)

Figure 2. (a) Initial electron density dependence on pressure in air for 150 fs pulse; (b) corresponding plasma density profiles for pressures 2, 3, 4 and 6 atm.

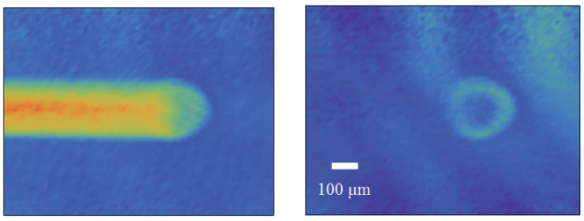

(a) (b)

Fig 1. Phase distortion corresponding to a) plasma channel; b) pulse propagation.

[1] V P Kandidov, S A Shlenov, O G Kosareva, "Filamentation of high-power femtosecond laser radiation", QUANTUM ELECTRON, 39 (3), 205–228 (2009)

[2] A. Couairon and A. Mysyrowicz "Femtosecond filamentation in transparent media," Physics Reports 441, 47 (2007).

[3] Abdollahpour D., Suntsov S., Papazoglou D. G., and Tzortzakis S. "Measuring easily electron plasma densities in gases produced by ultrashort lasers and filaments," Opt. Express..19 (18), 16866-16871 (2011)

[4] Théberge F., Liu W., Simard P. Tr., Becker A., and Chin S. L. "Plasma density inside a femtosecond laser filament in air: Strong dependence on external focusing ", Phys. Rev. E., 74 (3), 036406. (2006)

[5] La Fontaine, B., Vidal, F., Jiang, Z., Chien, C.Y., Comtois, D., Desparois, A., Johnston, T.W., Kieffer, J.-C., Pepin, H. "Filamentation of ultrashort pulse laser beams resulting from their propagation over long distances in air" Phys. Plasmas 6, 1615 (1999)

[6] Papazoglou D.G. and Tzortzakis S. "In-line holography for the characterization of ultrafast laser filamentation in transparent media" Appl. Phys. Lett., 93(4), 041120–041123 (2008)

[7] Bodrov S., Bukin V., Tsarev M., Murzanev A., Garnov S., Aleksandrov N. and Stepanov A. "Plasma filament investigation by transverse optical interferometry and terahertz scattering" Opt. Express., 19(7), 6829-6835 (2011)

[8] Takeda M., Ina H., Kobayashi S. "Fourier-transform method of fringe-pattern analysis for computer-based topography and interferometry" J. Opt. Soc. Am., 72 (1), 156-160 (1982)

[9] Nugent K. "Interferogram analysis using an accurate fully automatic algorithm" Appl. Opt., 24(18), 3101-3105 (1985)

Defects in Solid State Materials as a Result of Interaction with Charged Particles and High-Energy Photons and Their Applications for Radiation Detectors and Imaging on Nanometric Scale

A.P. Voitovich
Institute of Physics, National Academy of Sciences, 68 Nezalezhnosti Av. 220072, Minsk, Belarus, + 375 17 2841732, e-mail: a.voitovich@ifanbel.bas-net.by
R.M. Montereali
ENEA C.R. Frascati, Fusion and Technologies for Nuclear Safety and Security Dept., Photonics Micro- and Nanostructures Lab., 45 Via E. Fermi, 00044, Frascati, Rome, Italy
V.S. Kalinov, A.N. Novikov, L.P. Runets, A.P. Stupak
Institute of Physics, National Academy of Sciences, 68 Nezalezhnosti Av. 220072, Minsk, Belarus

Abstract: It is established that the peculiarities of the radiation imaging solid-state detectors can be exploited for X-ray micrograph and for observation of biological samples. It is shown that for many materials used in radiation dosimetry, nanocrystals have the larger range of linear response to dose compared with crystals of the same composition.

1. Introduction

Intrinsic point defects can be produced in different kinds of crystalline materials by extreme ultraviolet, X or gamma rays, electrons, ions or neutrons. Their dimensions are close to lattice spacing and lie typically in the range 0.5–2.0 nm for crystalline inorganic solids. These features combined with the peculiar properties of the hosting matrix are promising for use as efficient storage media with a high recording density as well as for direct writing of nanostructures and for radiation imaging at nanoscale. Moreover, formation of intrinsic defects in insulating crystals has been successfully applied for dosimetry of ionizing radiations. Their thermoluminescence (TL) is proportional to the absorbed radiation doses. Nanocrystals (NCs) could be considered as promising candidates for dosimetry detectors of improved performances.

2. Results

Direct writing with a focused monochromatic soft X-ray microprobe of fixed energy from 400 to 700 eV allows the realization of low-dimensional, nominally down to one hundred of nanometers, fluorescent arrays of lines and dots, based on active F_2 and F_3^+ color centers (CCs), in LiF crystals and thin films. In Fig. 1a the CLSM photoluminescence (PL) image of a regular array of light-emitting lines, directly written on a 0.3 μm thick LiF film on Si substrate, is shown together with its intensity profile (Fig. 1b). It consists of 8 lines regularly spaced by 3.5 μm, whose measured full-width at half-maximum is about 800 nm, a typical value easily achievable and detectable in standard operating microscope conditions. The fluorescence image, stored in the LiF film grown on a reflective substrate, was obtained by a CLSM (Nikon Eclipse 80i-C1) equipped with an Argon laser at 457.9 nm. Irradiation with blue light excites the visible PL of the F_2 and F_3^+ lattice defects locally created in the areas previously exposed to the incoming focused X-ray beam, which appear bright in the picture of Fig. 1a.

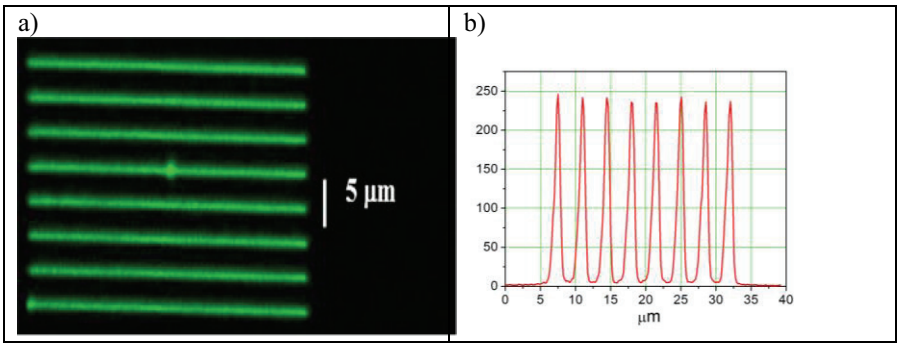

Fig. 1. PL grating based on F_2 and F_3^+ CCs and directly written by a 450 eV X-ray beam on a 0.3 μm thick LiF film grown on Si substrate (a). PL intensity profile of the light-emitting grating registered along a vertical line (b).

Figs. 2a,b show the soft X-ray micrographs of a dried dragonfly wing obtained on LiF thin films of equal thickness, about 1 μm, thermally evaporated on glass and Si (100) substrates, respectively. They were simultaneously exposed under vacuum with a single-shot of a Nd-YAG laser-plasma source with Cu target, whose penetration depth is comparable and/or higher than the total film thickness, at a soft X-ray fluence of ~ 350 $\mu J \cdot cm^{-2}$/shot. In the integrated PL images, the F_2 and F_3^+ signal intensities can be tentatively assumed to be proportional to the concentrations of active CCs, which are directly related to the X-ray transparency of the exposed sample; thus, the more absorbing parts of the biological object appear as darker. Also in this case, with the same acquisition parameters, the higher sensitivity of the LiF film on Si substrate with respect to the LiF film on glass is noticeable, and the higher optical contrast allows identifying smaller details.

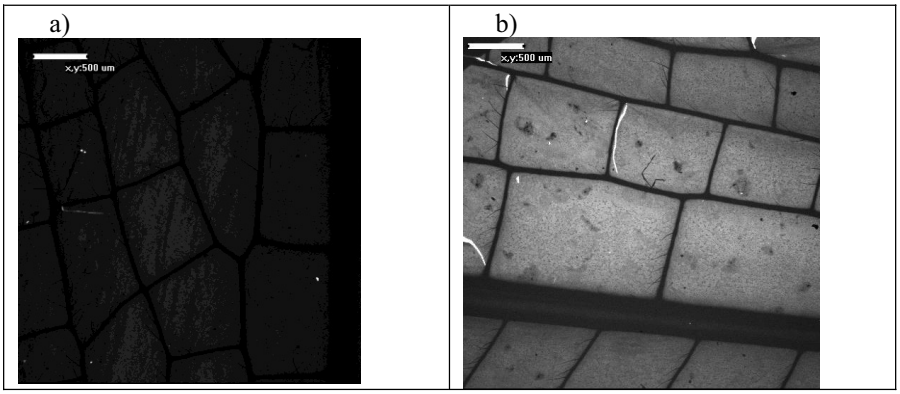

Fig. 2. CLSM fluorescence images of soft X-ray contact micrographs of a dried dragonfly wing stored on a 1 μm thick LiF film thermally evaporated on glass (a) and silicon (b). Bar length: 500 μm.

We consider also the characteristics of the optical absorption transitions, PL and photoluminescence excitation (PLE) spectra for the near-surface CCs (SCCs) in LiF. These centers were created in LiF NCs by gamma rays from a ^{60}Co source. NCs were produced by mechanical fragmentation of a nominally pure LiF monocrystal. PL and PLE spectra of SCCs which contain more than one anion vacancy differ strongly from the corresponding spectra of the bulk centers of the same composition. There are differences in the following characteristics between SCCs and CCs: (i) in the position of the energy levels and in the peak and width values of PL and PLE bands; (ii) in the magnitudes of the transition probabilities; (iii) in the parameters of the electron-phonon interaction. The depths of the electrons and holes traps will change moving from the crystal volume to its near-surface layer. All the differences listed above will be dominant in NCs due to their extended surface. They will change the characteristics of thermoluminescence (TL) of irradiated NCs compared to the bulk crystal. These effects stimulate research on the possibilities of using NCs for radiation dosimetry as the TL based techniques are widely used for measurements of ionizing radiation doses.

It is shown that temperature dependencies of TL intensities for crystals and NCs differ greatly. The ranges of radiation exposures with linear TL response are given for several nano- and microcrystals of doped insulating materials used as radiation detectors. It can be derived that these ranges are much larger for the nanocrystals in comparison with the microcrystals of the same composition. This behavior of the NCs is useful also for measurements of the heavy charged particles doses. Along with the wider range of linear response, many NCs exhibit negligible fading and good reusability. Thus, the NCs demonstrate good opportunities for use as detectors at high doses of ionizing radiation, including heavy charged particles.

3. Conclusion

The characteristics of the radiation imaging LiF detectors are particularly suitable for X-ray lensless imaging techniques, including contact microscopy as well as absorption and phase contrast tomography. Improvements of LiF film detector performances and optimization of the reading technique are currently under development.

SCCs with previously unobserved absorption and luminescence characteristics have been found in NCs produced by mechanical fragmentation of the LiF crystal. The absorption and PL spectra of SCCs are shifted toward longer wavelengths as compared with those for CCs of the same type in the bulk crystal. The PLE spectra for SCCs have two or three bands with not strongly various intensities. In near-surface layers of LiF crystals, the activation energy of the defects diffusion is significantly higher than in the bulk of the crystals. The NCs have good characteristics of linear response, fading and perspectives in order to be used as detectors of ionizing radiation, including heavy charged particles. Characteristics improvements of NCs for detecting ionizing radiation are currently under study.

Electric field fast measurement in pulse discharges at elevated gas pressure

S.N.Tskhai[1], S. Yatom[2], Ya. E. Krasik[2]
[1]P.N.Lebedev Physical Institute RAS, Moscow, 119991 GSP-1 Leninskii prosp., 53, Russia
[2] Department of Physics, Technion, Haifa 32000, Israel
e-mail: tskhai@lebedev.ru

Abstract: The possibilities of measuring the intensity of the electric field in high-pressure plasma with non-linear optics methods are studied. The measurements of the electrical field intensities dynamics in impulse discharges are presented.

The topic of plasma with near atmosphere density is related to multiple applications[1]. One of the main characteristics of plasma is the intensity of the electric field. While there are many methods of measuring it, in case of high density plasma, it seems only one method, based on non-linear optical interactions of the quasi-constant external and laser light electrical fields, remains viable [2]. The distinctive differences of the method are:

- Spatial resolution is defined by the necking area of the focused laser beam (~mm^3)
- The temporal resolution is defined by the length of the laser impulse, in [3] demonstrating experiment with 30 ps impulses.
- Not sensitive to the inhomogeneity of the particle density, this is achieved by normalizing the signal, that is generated with the external electrical field using the standard CARS signal, that is generated at the same time, and has the same dependence on the particle density.
- Analyzing the polarization plane of the radiation, generated with the electric field, it is possible to determine the direction of the field vector [4].
- Low sensitivity for plasma microfields is allowing to measure only the external electrical field in the gas-discharge plasma []5].

In the current work, the application of the method to analyzing impulse discharges hydrogen with pressures about ≥1 atm [6].

The work was supported by the Russian Scientific Foundation (project №14-22-00273).

[1] P. Bruggeman, R.Brandenburg, “Atmospheric pressure discharge filaments and microplasmas: physics, chemistry and diagnostics”, J. Phys. D: Appl. Phys. **46**, 464001 (2013)
[2] V.P.Gavrilenko, V.N.Ochkin, S.N.Tskhai, “Progress in plasma spectroscopic diagnostics based on Stark effect in atoms and molecules”, Proc. SPIE Vol 4460, 207-229, 2002
[3] B. Goldberg, I. Shkurenkov, I.V Adamovich S. O’Byrne, and W.R. Lempert, “Electric field measurements in a dielectric barrier nanosecond pulse discharge with sub-nanosecond time resolution”, Plasma Sources Sci. Technol. **24** 035010 (2015) (
[4] S. N. Tskhai, D. A. Akimov, S. V. Mitko, V. N. Ochkin, A. Yu. Serdyuchenko, D. A. Sidorov-Biryukov, D. V. Sinyaev and A. M. Zheltikov, “Time-resolved polarization-sensitive measurements of the electric field in a sliding discharge by means of dc field-induced coherent Raman scattering”, J. Raman Spectrosc.; **32**: 177–181 (2001)
[5] V.N. Ochkin, S.Yu. Savinov, S.N. Tskhai, Influence of microfields on coherent optics measurements of electric field intensity, J. of Russian Laser Research, **18** 582-590 (1997)
[6] S. Yatom, S. Tskhai,and Ya. E. Krasik, “Electric Field in a Plasma Channel in a High-Pressure Nanosecond Discharge in Hydrogen: A Coherent Anti-Stokes Raman Scattering Study”, Phys.Rev.Lett. **111** 255001 (2013)

“Femtosecond Pump-to-Probe Spectroscopy of primary events in photosynthesis”

*Dmitriy Cherepanov[1,2,3], Fedor Gostev[1], Mahir Mamedov[1,2], Ivan Shelaev[1], Alexey Semenov[1,2], Vladimir Shuvalov[1,2], Victor Nadtochenko[1]**

1 N.N.Semenov Institute of Chemical Physics Russian Academy of Sciences, Moscow, Kosigin str. 4, Moscow, 119991, Russia;
2 A.N. Belozersky Institute of Physical-Chemical Biology, Moscow State University, Moscow 119991, Russia;
3 A.N. Frumkin Institute of Physical Chemistry and Electrochemistry, Russian Academy of Sciences, Leninsky prospect 31, Moscow, Russia, 199071
*Corresponding author : E-mail: nadtochenko@gmail.com.

Abstract: The femtosecond pump-probe spectroscopy revealed the ultrafast charge separation in photosystem 1 with time constant 100 fs. This reaction of the primary charge separation is one of the fastest reactions in photobiology.

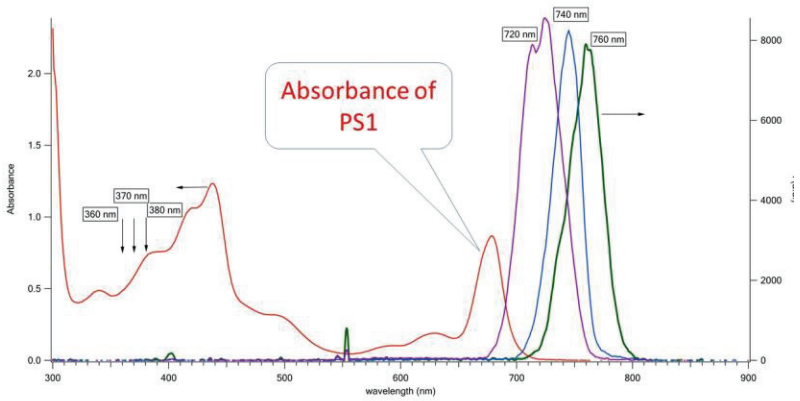

Figure 1. Absorbance spectrum of PS1 and spectra of femtosecond pump pulses centered at the red wing of the Qy band of PS 1. Wavelength corresponding to the two photon absorption are indicated.

The energy and electron transfer in photosystem I (PS I) from cyanobacteria *Synechocystis sp.* PCC 6803 was studied by femtosecond pump-probe absorption spectroscopy. The excitation was performed using ~22-25-fs laser pulses centered at 680 nm, 700 nm, 720 nm, 740 nm and 760 nm as shown in Figure 1. The transient spectra induced by the femtosecond pump pulse were detected in the time delay window from 20 ps to ~~of~~ 500 ps.

The main goal of the study was to clarify two important issues: 1) whether the formation of the primary and the secondary ion-radical pairs $P700^+A_0^-A_1$ and $P700^+A_0A_1^-$ in PS I can be formed under single-photon absorption at the far red edge of Q_Y band?;
2) what is a lifetime of the primary ion-radical $P700^+A_0^-A_1$ formation?

The effect of the pump pulse wavelength and the pump pulse power on the transient spectra was studied in detail. Transient spectra depend on the pump power. Detailed analysis of transient spectra shape as a function of the pump power energy shows that under red light excitation two channels of PS

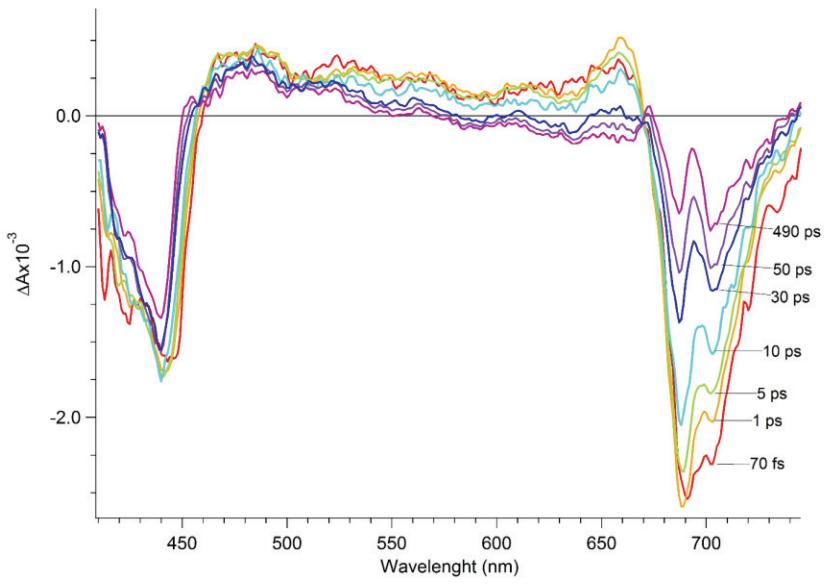

Figure 2. Transient absorbance spectra of PS 1 after 22fs laser pump with wavelength of 720 nm and pulse energy of 20 nJ.

I absorption can be realized: linear single photon absorption and nonlinear multiphoton absorption. The linear single photon absorption leads to the appearance of specific spectral features in the transient spectra shown in Figure 2. These spectral features are the bleach peaks at ~690 nm and ~705 nm. These bleach peaks correspond to the depletion of the ground state population of the primary electron acceptor A0 (690 nm) and primary electron donor P700 (705

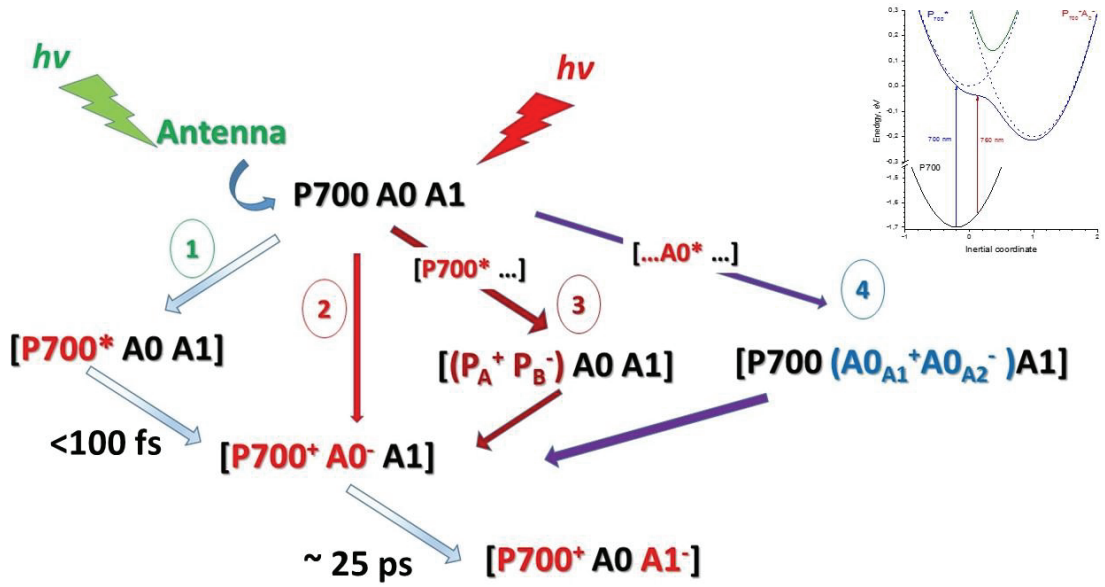

Figure 3. Possible routes of the primary charge separation in PS 1. Insert demonstrates the potential surface of the electron transfer between P700* and A0.

nm) at the initial time delays. These spectral features correspond to the transient spectra of $P700^+A_0^-A_1$ at the initial time delays (<~10ps) and $P700^+A_0A_1^-$ pairs for the longer time delays (~> 100 ps). The analysis of transient spectra corresponding to single photon absorption at short time delays reveals that formation of $P700^+A_0^-A_1$ occurs within 100 fs. The formation of the secondary radical pair $P700^+A_0A_1^-$ due to electron transfer between A_0 and A_1 has characteristic time close to 20 ps. The obtained femtosecond laser spectroscopy data evidences that the ultrafast formation of primary $P700^+A_0^-A_1$ ion-radical pair in PS I from *Synechocystis sp.* PCC 6803 occurs with characteristic time less than 100 fs. This process can be due to single photon absorption by reaction center of PS I even when the reaction center of PS I is excited by low-energy photons into the far-red edge of Q_Y absorption band. Figure 3 shows possible routes of the primary charge separation in PS 1. The route #1 is the formation of the electron excited state of P700 and following electron transfer. The route #2 suggests the direct photon absorption in the charge transfer state of $P700^+A_0^-A_1$. The route #3 relates to the charge separation between two chlorophylls in the dimer P700 and the following electron transfer to A0. The route #4 corresponds to the charge separation between two chlorophylls in the dimer A0 and following transfer of hole to the P700. The analysis of transient spectra when pump is at the red wing of Qy band and antenna pigments are almost not excited reveal that the route # 1 as it was suggest recently [1] is realized. The probability of routes # 2,3 and 4 is negligible small.

The work was supported by the Russian Science Foundation (grant 14-14-00789)

References.

1. Shelaev,I.V., F.E.Gostev, M.D.Mamedov, O.M.Sarkisov, V.A.Nadtochenko, V.A.Shuvalov, and A.Y.Semenov. “Femtosecond primary charge separation in Synechocystis sp PCC 6803 photosystem I.” Biochimica et Biophysica Acta-Bioenergetics **1797**, 1410-1420 (2010).

Dynamics of Photoinduced TICT-process for Thioflavin T in n-Alcohols

V. Stsiapura,[1] O. Bouganov,[2] S. Tikhomirov[2]
[1]Yanka Kupala State University, Grodno, Belarus; [2]Institute of Physics, National Academy of Sciences of Belarus, Minsk, Belarus
stsiapura@gmail.com, o.buganov@ifanbel.bas-net.by, s.tik@ifanbel.bas-net.by

Abstract. It has been established earlier that fluorescence quantum yield of Thioflavin T (ThT) – a probe widely used for amyloid fibrils detection – is viscosity-dependent and photophysical properties of ThT can be well-described by the fluorescent molecular rotor model, which associates twisted internal charge transfer (TICT) reaction with the main non-radiative decay process in the excited state of the dye. Solutions of ThT in 1-propanol, 1-pentanol, and 1-hexanol were studied using femtosecond transient absorption spectroscopy methods and we showed that solvent viscosity was the main factor that influenced TICT rate for ThT in alcohols.

Photophysical properties of Thioflavin T (ThT) have received much attention due to extensive use of this fluorescent probe for detection of amyloid fibrils [1, 2] – insoluble protein aggregates - related to several neurodegenerative disorders. It has been established that fluorescence quantum yield Φ of ThT is highly dependent on viscosity/temperature ratio η/T [3, 4] and the dye exhibits photophysical properties that are typical for fluorescent molecular rotors. In accordance with the molecular rotor model, a twisted internal charge transfer (TICT) process coupled to a twisting movement along C-C bond between benzthiazole (BTZ) and dimethylaniline (DMA) fragments (Fig.1) takes place in the excited state and represents the main non-radiative deactivation channel. In non-viscous media TICT process rate is considerably higher than of the radiative transition and majority of photoexcited ThT molecules deactivates via non-radiative TICT process. However for ThT in highly viscous media or when bound to amyloid fibrils the twisting rate decreases substantially and radiative transition becomes the major route of the excited state deactivation which explains dramatic enhancement of ThT fluorescence intensity.

Earlier it was reported [5] that for ThT in longer alcohols (1-butanol and 1-pentanol) TICT rate became independent of the molecular character of the solvent and was determined solely by viscosity values, i.e. twisting rate of the molecular rotor could be described as a process limited by rotational diffusion of ThT fragments

$$k_{TICT} = \frac{k_B T}{3\eta V_{ThT}}, \qquad (1)$$

where V_{ThT} – effective hydrodynamic volume of ThT twisting fragments, k_B – Boltzmann constant.

In this work femtosecond transient absorbance method was used to study solvent effect on TICT dynamics for ThT solutions in longer n-alcohols. Transient absorption measurements in subpicosecond and picosecond time domains were carried out in a 0.5 cm quartz cell using a home-made original femtosecond spectrometer, described elsewhere. Fluorescence quantum yields of ThT in alcohols were measured using coumarin 1 in ethanol as a standard.

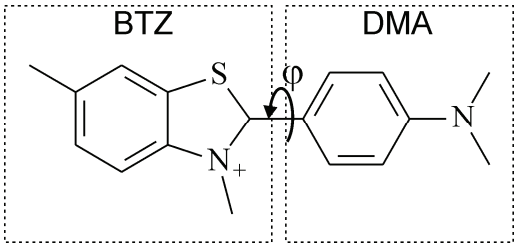

Figure 1. Scheme of Thioflavin T cation. Fragments of benzothiazole (BTZ) and dimethylaniline (DMA) are shown in boxes.

Sub-picosecond time-resolved absorption spectra for ThT in several n-alcohols (1-propanol, 1-pentanol, 1-hexanol) were measured. Fig.2 shows dynamics of transient absorption spectra of ThT in 1-pentanol after excitation with pump pulse at 400 nm. Transient absorption spectra of ThT in all studied solvents have similar behavior: besides the bleaching band (negative signal in 420-440 nm range) related to depopulation of the ground state of the dye one can see rise and decay of gain band (negative signal in the spectral range of 450-600 nm) and induced absorption bands at 470 and 720 nm.

In accordance with earlier reported data [6] we assign the induced absorption band at 720 nm to an absorption from emissive LE-state and the one at 470 nm – to an absorption from the dark TICT-state. Intense peak of the gain band at 490-500 nm is attributed to radiative transition from LE to the ground S_0-state.

Transient absorption curves were fitted using a set of exponentials convolved with the pump-probe correlation function. We found that kinetic curves in the range 480-580 nm for each solvent can be fairly well described using biexponential model (Table 1). The short-lived component with negative pre-exponential factor was assigned to emission from LE-state and the long-lived component - to absorption from TICT-state. Due to quite strong dependence of LE-state lifetime on probe wavelength within 480-580 nm range it is difficult to make quantitative conclusions and we can state that LE-TICT transition rate in the studied alcohols is in qualitative agreement with Eq. (1). It is noteworthy that fluorescence quantum yield values $\Phi \approx k_r / k_{TICT}$, where k_r – radiative rate constant, could be fairly well described by diffusion-limited process of twisting motion in ThT.

Table 1. Fluorescence quantum yield Φ and kinetics parameters for transient absorbance of ThT at 500 nm in alcohols at room temperature

solvent	Viscosity η, mPa·s at 298 K	Dielectric constant ε	pre-exponential factor α_1	τ_1, ps	pre-exponential factor α_2	τ_2, ps	$\Phi/10^{-4}$
1-propanol	1.945	20.1	-1.00	6.2±0.1	0.15	56±4	26
1-butanol	2.544	17.5	-1.00	8.2±0.7	0.20	>200 ps	43
1-pentanol	3.425	14.7	-1.00	12.9±0.3	0.08	>200 ps	63
1-hexanol	4.596	13.1	-1.00	22.0±0.8	0.06	>200 ps	88

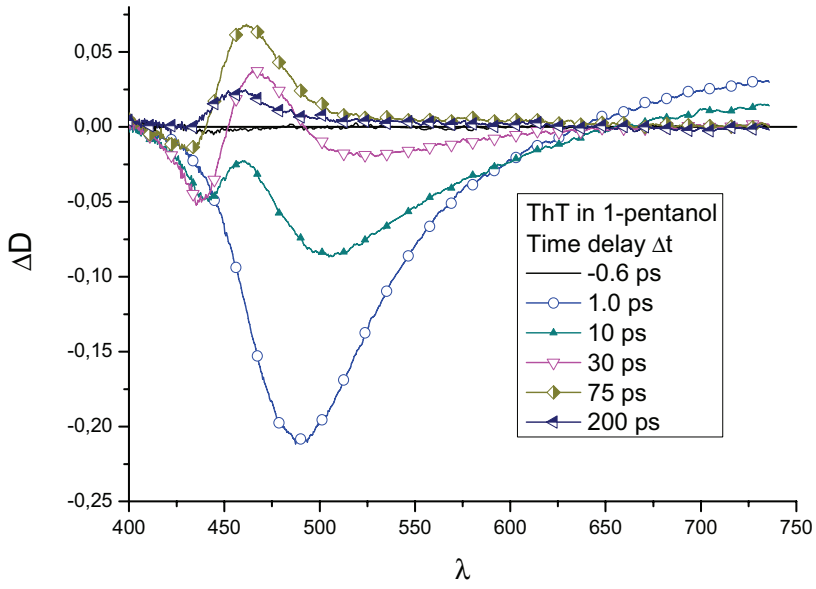

Figure 2. Transient absorbance spectra of ThT in 1-pentanol. λ_{ex} = 400 nm.

[1] Groenning, M., "Binding mode of Thioflavin T and other molecular probes in the context of amyloid fibrils-current status". J Chem Biol. **3**(1), 1-18 (2010)

[2] LeVine III, H., "Quantification of beta-sheet amyloid fibril structures with thioflavin T", Methods in enzymology, **309**, 274-284 (1999)

[3] Stsiapura, V.I., et al., "Thioflavin T as a Molecular Rotor: Fluorescent Properties of Thioflavin T in Solvents with Different Viscosity" J Phys Chem B. **112**(49), 15893-15902 (2008)

[4] Amdursky, N., Y. Erez, and D. Huppert, "Molecular rotors: what lies behind the high sensitivity of the thioflavin-T fluorescent marker". Accounts chem research. **45**(9), 1548-1557 (2012)

[5] Erez, Y., et al., "Temperature and Viscosity Dependence of the Nonradiative Decay Rates of Auramine-O and Thioflavin-T in Glass-Forming Solvents", J Phys Chem A, **116**(49): 12056-12064 (2012).

[6] Stsiapura, V.I., et al., "Charge transfer process determines ultrafast excited state deactivation of thioflavin T in low-viscosity solvents". J Phys Chem A. **114**(32), 8345-50 (2010)

Speeded up lifetime testing technique for streak tubes

A.Yu. Sokolov, P.I. Konovalov, M.P. Vikulin

Dukhov Research Institute of Automatics (VNIIA), 22, ul. Sushchevskaya, Moscow 127055, Russia

Abstract: Here presented the results of investigation of sensitivity variations during operational time of a streak tube produced by FSUE “VNIIA”. It showed that sensitivity decrease can be accurately characterized by an exponential function with an absolute term and a correction, which resulted from steak tube photocathode recovery processes. Here described the developed speeded up testing technique for streak tubes which uses principle of temporal regression of this function. The results of the experiment also allowed to identify dominating physical processes causing degradation of photocathode.

MCP PMT with high time response and linear output current for neutron time-of-flight detectors

A.S. Dolotov, P.I. Konovalov, R.I. Nurtdinov, M.P. Vikulin

Dukhov Research Institute of Automatics (VNIIA), 22, ul. Sushchevskaya, Moscow 127055, Russia

Abstract: A microchannel plate (MCP) photomultiplier tube (PMT) with a subnanosecond time response and a high linear output current has been developed. PMT is designed for detection of weak pulses of radiation in UV-, visible and nearer-IR ranges and can be used in neutron time-of-flight (nTOF) detectors in experiments on laser compression of thermonuclear fuel. The results of measurements of MCP PMT main parameters: photocathode spectral sensitivity, gain, maximum linear output current and time response - are presented.

Femtosecond Interferometry as a Tool for Optimal Control of Ions Photofragmentation.

Mikhail V. Korolkov (a) , Karl-Michael Weitzel (b)
(a) B.I. Stepanov Institute of Physics, National Academy of Science, Minsk, 220072 Belarus korolkovmv@Yahoo.com
(b) Fachbereich Chemie, PhilippsUniversität Marburg, Marburg. 35032

Abstract: The possibility to control of the ion photofragmentation process by means of varying of the time delay between two interfering femtosecond laser pulses with proper carrier envelope phases have been studied.

The control of the molecular bond breaking dynamics on the femtosecond time scale has received tremendous interest in recent years [1–7]. Much experimental and theoretical work has been devoted to manipulating nuclear and electronic wave packets [8–11]. In many cases two or even more wave packets are operative and may exhibit interference effects. The quantum interference of wave packets has attracted by now considerable attention [8–11].

Here we present our results of the study of ion photofragmentation process originating in interference field of two femtosecond laser pulses shifted in time. The idea of optimization of photofragmentation process is based on the fact that the resultant interference field and its envelope shape depend on the carrier envelope phase of each pulse and time delay between pulses. Mutual effect of time delay and the carrier envelope phases is caused by the formation of the transition state of vibrational wave packet by the first laser pulse. This wave packet localized in the vicinity of eigenenergies of few vibrational states and moving in the ground electronic state and by the beginning of the second pulse defines initial conditions for the fragmentation under action of second pulse. As a result the photofragmentation dynamics essentially depends on the time delay of the second pulse and it's carrier phase and substantially complicates the vibrational dynamics of wave packets in each of the electronic states, inducing transitions between them in the wide range of D-Cl distance from near-equilibrium states of nuclei to a state of almost complete dissociation [12,13]. We have demonstrated that the using of interference field of two time-shifted coherent laser pulses is a powerful tool that provides additional possibility to control the fragmentation process and the mixing processes electronic and nuclear dynamics [13, 14].

The photodissociation of DCl+ ions has been investigated within the frame of wavepacket calculations based on the numerical solution of coupled time-dependent Schrödinger equations. The procedure has been described extensively in previous publications [15-16]. Here, only the most important aspects necessary for the understanding of the results are reiterated. As in previous work we concentrate on the influence of three different electronic states, the X $^2\Pi$ (channel 1); 2 $^2\Pi$ (channel 2); and 3 $^2\Pi$ (channel 3). More specifically we have solved the following three coupled time-dependent Schrödinger equations for the nuclear wave functions Ψ j(r, t) of the electronic ground state (j = X), as well as the first and second excited electronic $^2\Pi$ states (j = 2Π, 3Π) [15]. The electric field is linearly polarized and parallel to the ion axis caused by two laser pulses:

$$E_L(t) = E_0 \cdot \sin^2\left(\pi t / t_p\right) \cdot \cos\left[\omega_0 t + \varphi_1\right] + E_0 \cdot \sin^2\left(\pi (t - t_0) / t_p\right) \cdot \cos\left[\omega_0 (t - t_0) + \varphi_2\right] \quad (1)$$

The set of time dependent Schrödinger equations [12] have been solved numerically with time steps of 1 atomic unit (≈ 24 as)..

At Fig. 1 we present few (obtained for the combinations of the CEP {φ1; φ2}: {0;0}, {0;π/2}, {0;π}, and {0;3π/2}) femtosecond interferograms calculated for pulses of 7 fs (FWHM) duration at 800 nm. The peak intensity of a single laser pulse was 8.96× 1014 W/cm2 (E_0 = 0.16 a.u.). $W(\Delta t) = \int |E_L(t_0=\Delta t)|^2 dt$. For $\Delta t > t_p$ we have non overlapping regime with W(Δt)=const, see Fig. 2. We can clearly distinguish a regime with intensity driven dynamics ($t \le 7$ fs) and a regime with revivals of nuclear (vibrational) wavepackets (t > 15 fs). There is also a transitional regime, which we have dubbed mutual electron-nuclear dynamics regime [14]. The results presented clearly demonstrate that the ratio of product yields D+ : Cl+ can be manipulated from about 7 : 1 to 1 : 7 by means of simply changing the time delay and/or the CEP We speculate that even more extensive control could possibly be achieved by applying pulse shaping techniques. Time dependence of populations in the regime of non-overlapping pulses

The interferograms given above present the yields at the end of the laser-molecule interaction. In order to gain additional insight into the molecular dynamics it is helpful to look at the time dependence of the relevant populations. At Fig.2 the time dependence of populations of vibrational eigenstate and product yield of ions are presented for the case of non-overlapping regime (delay time $\Delta t > t_p$) Here we use the CEP combination φ1=φ2=0 for t_{FWHM} = 20 fs at 2.13μm. Note, this occurs in the non-overlapping regime and for the intermediate time 55fs < t < 75fs all populations is constant< but the nuclear wave packet moving in the ground electronic state and create the initial conditions for the photofragmentation process stimulated by second laser pulse. The spatial position of the nuclear wave packet in the

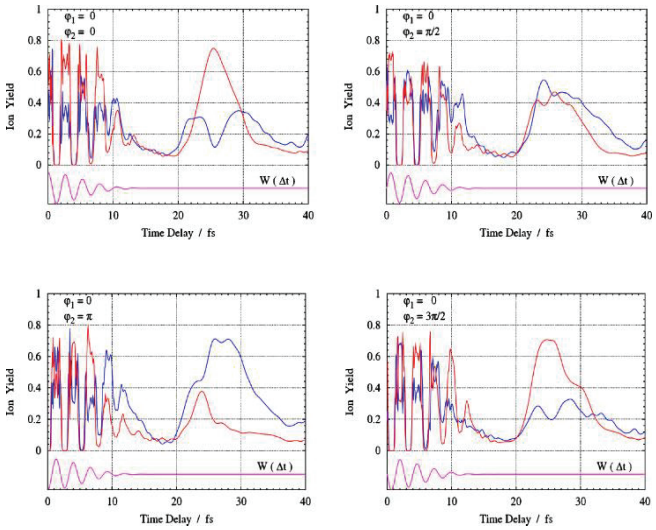

Fig.1 Product yield as function of time delay between two 7fs pulses with four CEP combination.

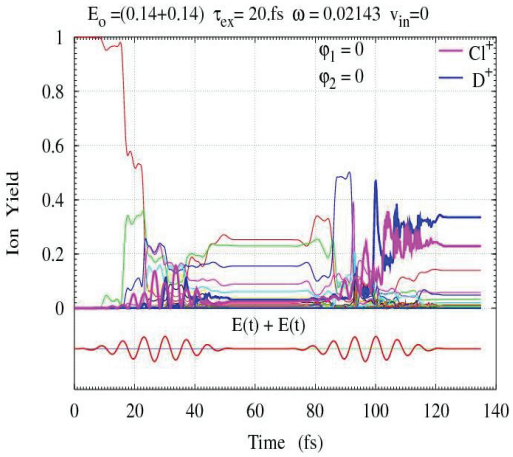

Fig.2 None overlapping regime. After the first laser pulse a set of vibrational eigenstates arise in the electronic ground state and create the initial conditions for the second part of fragmentation (here v=0, 1,…,5 are exited enough).

ground electronic state and the CEP of the second laser pulse will determine final efficiency of the fragmentation process. The overall dynamics is much more complex and have to take into acount the mixing of electronic and nuclear dynamic.

[1] A. H. Zewail, "Femtochemistry: Atomic-Scale Dynamics of the Chemical Bond," J. Phys. Chem. **104**, 5660-5694 (2000).

[2] S. Rice and M. Zhao, Optimal Control of Molecular Dynamics (Wiley, New York, 2000), 437 p.

[3] F. Krausz ,and M. Ivanov, "Attosecond physics," Rev. Mod. Phys. **81**, 163–234 (2009).

[4]. T. Brixner and G. Gerber, "Quantum control of gas-phase and liquid-phase femtochemistry," Chem. Phys. Chem. **4**, 418 (2003).

[5]. V. V. Lozovoy, X. Zhu, T. C. Gunaratne, D. A. Harris, J. C. Shane, and M. Dantus, "Control of molecular fragmentation using shaped femtosecond pulses," J. Phys. Chem. A **112**, 3789 (2008).

[6] P. den Hoff, I. Znakovskaya, M. F. Kling, and R. Vivie-Riedle, "Attosecond control of the dissociative ionization via electron localization: a comparison between D(2) and CO," Chem. Phys. **366**, 139 (2009).

[7] Q. Su, Y. Han and S. Cong, "Quantum control of multi-photon dissociation of HCl+ with intense femtosecond laser pulses," J. Chem. Phys. **138**, 024304 (2013).

[8] K. Ohmori, "Wave-packet and coherent control dynamics," Ann. Rev. Phys. Chem. **60,** 487 (2009)

[9] M. V. Korolkov, J. Manz, and G. K. Paramonov, "Theory of ultrafast laser control for stateselective dynamics of diatomic molecules in the ground electronic state: Vibrational excitation, dissociation, spatial squeezing and association," Chem. Phys. 217, 341-374 (1997).

[10] J. A. Cina, "Wave-packet interferometry and molecular state reconstruction: Spectroscopic adventures on the left-hand side of the Schrödinger equation," Ann. Rev. Phys. Chem. **59,** 319 (2008)

[11] H. Katsuki, H. Chiba, C. Meier, B. Girard, and K. Ohmori, "Wave packet interferometry with attosecond precision and picometric structure," Phys. Chem. Chem. Phys. **12,** 5189 (2010).

[12]M. V. Korolkov and K.-M. Weitzel, Carrier Envelope Phase Effects in Photofragmentation: Orientation Versus Alignment," Opt. Spectrosc. 111, 606-617 (2011).

[13] M. V. Korolkov and K-M. Weitzel, "Femtosecond Interferometry of Molecular Dynamics – the Role of Relative and Absolute Phase of Two Individual Laser Pulses," Zeitschrift fuer Physikalische Chemie. **225**, 1073–1088 (2011).

[14] M.V. Korolkov and K.-M. Weitzel, "Control of competing dissociation channel by femtosecond interferometry: aspects of electron and nuclear dynamics," Chem. Phys. Letters. 48, 209-213 (2010).

[15] M. V. Korolkov and K-M. Weitzel, "On the control of product yields in the photofragmentation of deuteriumchlorid ions (DCl+)," J. Chem. Phys. 123, 164308 (1-8) (2005).

[16] M. V. Korolkov and K.-M. Weitzel, "Laser pulse control of photofragmentation in DCl^+: The effect of carrier envelope phase," Chem. Phys. **338,** 277-284 (2007).

Numerical simulation of temperature dynamics in TiAlN thin films on Si subtsrate under nanosecond laser irradiation

G.D. Ivlev, O.R. Ludchik
Belarusian State University, 4, Nezavisimosti avenue, 220030 Minsk, Republic of Belarus
E.I.Gatskevich
Belarusian National Technical University, 65, Nezavisimosti avenue, 220013 Minsk, Republic of Belarus
e-mail:gatskevich_elena@yahoo.com

The thin films of binary nitride TiAlN are used as wear-resistant strengthening layers in technology of production of cutting tools and protective coating. Earlier [1] we carried out experimental study on the effects of the modification of thin film TiAlN on Si substrate under irradiation by intensive nanosecond pulses of a ruby laser. It was found that laser-induced processes in TiAlN leads to change in film morphology. At that specific changes in reflectivity at the wavelengths of probing beam are observed. The object of this investigation is to clarify the laser-induced processes under laser influence on TiAlN/Si by use of numerical simulation, and also to determine the temperature regimes at which laser effect on film leads to modification of structures state of TiAlN film and observed reflectivity dynamics.

The modelling was carried out on the basis of the numerical solution of thermal problem in one - dimensional approximation by finite difference method for experimental conditions [1]. In calculation we used the implicit scheme and tridiagonal matrix algorithm. The temporary form and duration of laser pulse (70 ns on level 0.5) corresponded to the experiment. The calculations were led for sample TiAlN/Si with nitride film thickness 0.5 μm. The data about space-time evolution of temperature in heated up layer of the system TiAlN/Si are received at a series of laser irradiation energy density W. At $W \leq 0.5$ J/cm^2 the calculated peak temperature reaches 1640 K at the surface and 1020 K at film/substrate interface. In this regime of irradiation any change in the film morphology is not observed.

With W increase up to 0.6 J/cm^2 morphological changes in the film take place. The formation of the system of lateral cells of micron sizes (on the average 1.8 μm) exceeding TiAlN film thickness is observed. And the average size of cells decreases approximately to 2 times with increase W up to 0.8 -0.9 J/cm^2.

Observable transformation of the structure/morphology of the film results from relaxation processes occurring in the area of significant thermostimulated mechanical stresses which are caused by very high temperature gradients in the film during laser pulse. In the conditions of laser irradiation with energy density 0.8 J/cm^2 the calculated peak values of temperature reach 2320 K (film surface) and 1580 K (film/substrate interface). If $W \geq 1$ J/cm^2, destruction and partial or total removal of the TiAlN film take place owing to ablation [1], which is reached at calculated surface temperature about 2800 K. In considering range of energy density the dependences of peak temperature at the film surface and film/substrate interface are practically linear.

Aggregate result of this work is the numerical solution of thermal problem with regard to particular experimental situation and description of space-time evolution of temperature in thin-film system TiAlN/Si under nanosecond ruby laser irradiation in different energy regimes resulting in the changes in morphology of the film of binary nitride.

[1] Ivlev G.D., Zaikov V.A., Klimovich I.M., Ludchik O.R. Interactions of radiation with solid. Proceeding of 11 International conference. Minsk, 23-25 September 2015. P.33-35.

Dynamics of nanopulsed laser annealing of thin film germanium

G.D. Ivlev, S.L. Prakopyev,
Belarusian State University, 4, Nezavisimosti avenue, 220030 Minsk, Republic of Belarus
E.I.Gatskevich
Belarusian National Technical University, 65, Nezavisimosti avenue, 220013 Minsk, Republic of Belarus
e-mail:gatskevich_elena@yahoo.com
R.I. Batalov, R.M. Bayazitov, I.A. Faizrakhmanov
Physical-Technical Institute of the Russian Academy of Sciences, Sibirsky tract, 10/7, 420029 Kazan, Russia

Germanium is a promising material to develop effective light emitters in infrared spectrum (1.5-1.6 μm). Unfortunately, the efficiency of such emitters and laser structures is low and methods of their creation (for example, molecular beam epitaxy) are expensive. The alternative method of formation of n-type tensile strained Ge layers can be vacuum deposition of Ge films and following nanosecond laser annealing.

In this paper laser-induced processes in heavily n-doped germanium films on semiconducting and insulating substrates have been studied by methods of time-resolved reflectivity measurements and numerical simulation. The n-Ge:Sb thin amorphous films are produced using the ion-beam sputtering on p-Ge, p-GaAs and fused silica (α-SiO_2) substrates. The samples were irradiated by ruby laser pulses. The pulses were of a nearly Gaussian temporal shape with full width at half maximum being 70 ns. Owing to generation of numerous modes, a high uniformity of energy distribution over the laser-irradiated zone on the sample surface was achieved. The spatial variation in the energy density W over the laser spot of 4 mm in diameter was less than ± 5 %. The W value changed from 0.4 to 1.0 J/cm^2 by using calibrated neutral filters.

The in-situ monitoring of the ruby laser-induced processes in the samples was realized by using a nonspiking pulsed Nd:Glass laser as a probing radiation source and KDP for frequency doubling, i.e. the probing beam consisted of two harmonics with λ_1=1.06 and λ_2= 0.53 μm.

The differences in reflectivity dynamics R(t) are observed for the samples with semiconducting and insulating substrates. It is known the solid ↔ melt phase transition in Ge is the semiconductor ↔ liquid metal transition. Liquid metal is characterized by the high values of reflectivity thus the duration of high R corresponds to melt duration τ_m. The subsequent falling of reflectivity takes place at the final stage of crystallization. The time of falling τ_d is much longer under solidification of Ge films on insulating substrates then the same on semiconducting one.

The time τ_d characterizes the velocity V_c of the solidification of Ge at the final stage of phase transition. In the situation of laser annealing of single Ge and Si, V_c decreases with the approach the surface by epitaxial crystallization front. This decrease is connected with the diminishing of temperature gradient near interface. In epitaxial processes τ_d should grow with τ_m(W) increase. We observed this on the dependences of $\tau_d(\tau_m)$ corresponding to Ge and Si. In experiments with n-Ge:Sb on p-GaAs and on Ge substrates we observe that τ_d does not rise with W increase (and also with τ_m increase), more over the time of falling may decrease.

In order to clarify the experimental data, the numerical simulation of laser-induced transformations has been carried out. Temperature distribution was determined on the basis of numerical solution of Stefan problem. The reasonable agreement is obtained between calculated melt duration and experimental data from time-resolved reflectivity measurements. The threshold energy densities at which the onset of melting of the film and the substrate takes place, are determined.

Stabilization CEO of Kilohertz Solid-State Laser System for Attosecond Pulses Generation Experiments

A.V. Kirpichnikov[1], V.V. Petrov[1,2,3], G.V. Kuptsov[1,3], A.V. Laptev[1], V.A. Petrov[1,2], E.V. Pestryakov[1], V.I. Trunov[1],

[1]Institute of Laser Physics SB RAS, Novosibirsk, Russia
[2]Novosibirsk State Technical University, Novosibirsk, Russia
[3]Novosibirsk State National Research University, Novosibirsk, Russia
vpetv@laser.nsc.ru

Abstract: A carrier-envelope offset phase stabilization (CEO) system was developed and implemented. It is allowing one to achieve residual instability ~0.17 radian (rms) for the 30 fs-pulse. It is sufficient to generate attosecond pulses efficiently.

The design and creation of femtosecond laser systems with high intensities are one of the most important trends in laser physics. Laser facilities with the intensity reaching the level of 10^{25} W/cm^2 or higher open a way to the experimental research in the wide range of problems in fundamental physics, chemistry, biology and their applications [1].

Obtaining one or more of attosecond light pulses opens the possibility of coherent control of electronic processes in the attosecond time scale [2]. Although attosecond pulses train is obtained relatively easy through high harmonic generation process in gases, the generation of a single attosecond pulse requires more complex laser systems with either polarization gating, dual-frequency mixing or spatial filtering. Common to all these methods is the stabilization of the carrier-envelope offset phase, which allows optimizing the electric field shape of the radiation to generate one or two pulses [3]. Despite intensive research in leading scientific centers worldwide, the subject is far from finished.

In this work, we concentrated attention on the study of the characteristics of all solid-state femtosecond laser system consisting of a master oscillator and a multi-pass amplifier, for further shortening of the pulse duration in a nonlinear medium. A mirror-dispersion controlled oscillator generates broadband (~100 nm), ultrashort (~10 fs) pulses at ~75 MHz repetition rate. The pulses are stretched by traversing a suitable amount of optical glass to a safe value of intensity for amplification. Third-order dispersion pre-compensation is achieved by a certain number of reflections from TOD-dispersion compensating mirrors. Then the pulses are amplified by 9- passes through a 1 kHz-pumped amplifier assembly to ~ 0.6 mJ. After the first four passes a single pulse is selected from the MHz-pulse train to be further amplified in another five passes. After amplification the pulses are recompressed to less than 30 fs by a double-prism compressor, central wavelength – 800 nm.

An oscillator carrier-envelope offset phase stabilization system was implemented. In general, the spectral components of radiation emitted from the femtosecond laser cavity have non-zero offset leading to different phase shifts, as envelope moves with the group velocity and carrier moves with the phase velocity. To measure the offset, spectrum is generated broader than an octave in a nonlinear fiber, and then red wavelengths are frequency doubled and are beaten with blue components.

The beat signal is rectified by a photodetector, an electronic unit selects the beat frequency and provides feedback to stabilize the frequency shift, which is calculated by the beat frequency. The control element of feedback loop is the acousto-optic modulator, which reduces the pump power of the master femtosecond oscillator.

To improve the circuit parameters the stabilization is performed at the frequency equal to one quarter of the pulse repetition rate. This leads to the fact that only every fourth pulse repeats with the same phase. During further amplification it is used lower pulse repetition rate, and if the frequency divider factor is set to 4, all output pulses have the same phase of the carrier-envelope offset.

The compensation circuit for carrier phase shift in the amplifier was created and experimentally verified. Phase perturbations during the amplification are registered in a nonlinear f-2f interferometer. The emission spectrum is broadened in the sapphire plate. The red part of the spectrum is doubled in a nonlinear crystal and is beaten with a blue part of the spectrum at the input of the spectrometer. Perturbation phase is calculated by

computer using the spectral beats recorded by the spectrometer. A signal proportional to carrier phase perturbations in the amplifier with a proper sign is mixed with the carrier phase drift signal of the master oscillator and used to control acousto-optic modulator's power (Fig. 1).

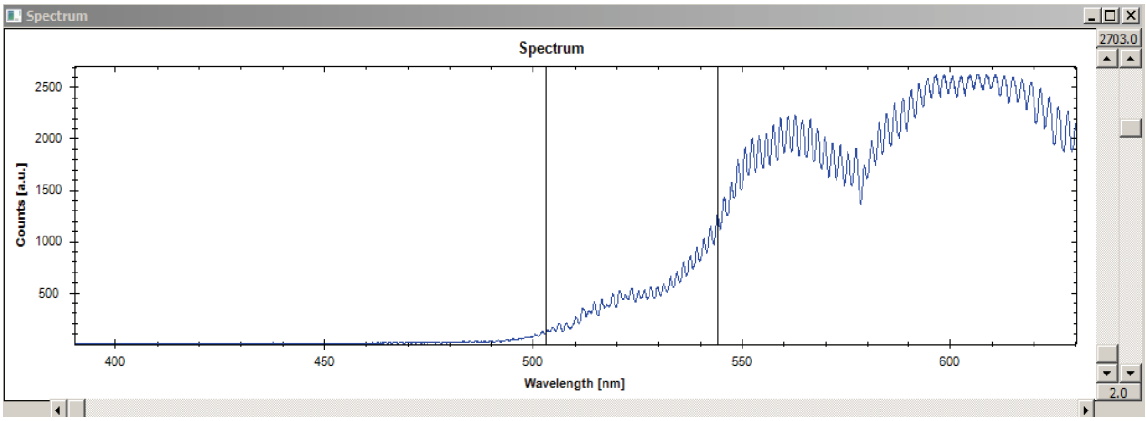

. The measured CCD spectrum of beats.

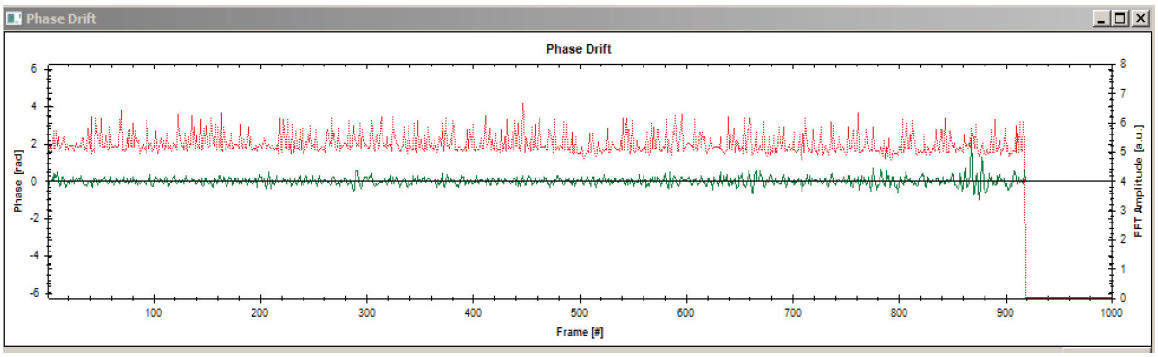

Fig. 2. Phase drift over time (green line). Phase drifts are calculated from the FFT data and averaged over the phase calculation window and the cycle time. The red line shows the FFT amplitude over time.

The stabilization system implemented has allowed one to achieve phase residual instability ~0.17 radian (rms) for the 30 fs-pulse, which is sufficient to generate attosecond pulses in forthcoming experiments efficiently (Fig. 2).

This work is supported in part by RAS Program "Extreme laser radiation: physics and fundamental applications", registration number AAAA-A15-115113010002-9 and Government program, registration number 01201374306.

[1] V.V. Petrov, E.V. Pestryakov, A.V. Laptev, V.A. Petrov, G.V. Kuptsov, V.I. Trunov, S.A. Frolov, Multiterawatt femtosecond laser system with kilohertz pulse repetition rate, QUANTUM ELECTRONICS, **44**, 452–457 (2014).
[2] M. Schultze, A. Wirth, I. Grguras, M. Uiberacker, T. Uphues, A.J. Verhoef, J. Gagnon, M. Hofstetter, U. Kleineberg, E. Goulielmakis, F. Krausz, State-of-the-art attosecond metrology, Journal of Electron Spectroscopy and Related Phenomena, **184**, 68–77 (2011).
[3] Pengfei Lan, Eiji J. Takahashi, and Katsumi Midorikawa, Optimization of infrared two-color multicycle field synthesis for intense-isolated-attosecond-pulse generation, PHYSICAL REVIEW A **82**, 053413 (2010).

Processing of Fiber Optic Bragg Sensor Signal by Fiber Bragg Gratings Filters

O.V. Butov*, A.A. Chertoriyskiy, O.V. Ivanov, A.M. Nizametdinov, V.L. Vesnin
*Kotelnikov Institute of Radioengineering and Electronics of Russian Academy of Sciences
Russia, 125009, Moscow, Mokhovaya, 11-7
Ulyanovsk Branch of the Kotelnikov Institute of Radioengineering and Electronics of Russian Academy of Sciences
Russia, 432071, Ulyanovsk, Goncharova str, 48/2
E-mail: ufire-spectrum@yandex.ru

Abstract: A system of signal processing for the fiber optic Bragg sensor using two Bragg gratings filters is proposed. The structural scheme of this system is described. The results of experiment with registration of metal plate oscillations excited by the impact of bullet are shown.

Fiber optic Bragg sensors (FOBSs) have applications in different areas of science and engineering, in particular, for control of deformations and vibrations. Although FOBSs are cheap, wide application of FOBSs is restricted by high cost of signal processing systems for these sensors. As a rule, such processing systems are based on polychromators [1-3] or tunable lasers [4].

As cheaper alternative, we propose to use two Bragg gratings filters, whose spectra have maxima shifted relative to the maximum of the reflection spectrum of the Bragg grating sensor [5]. The scheme of this signal processing system is shown in Fig. 1.

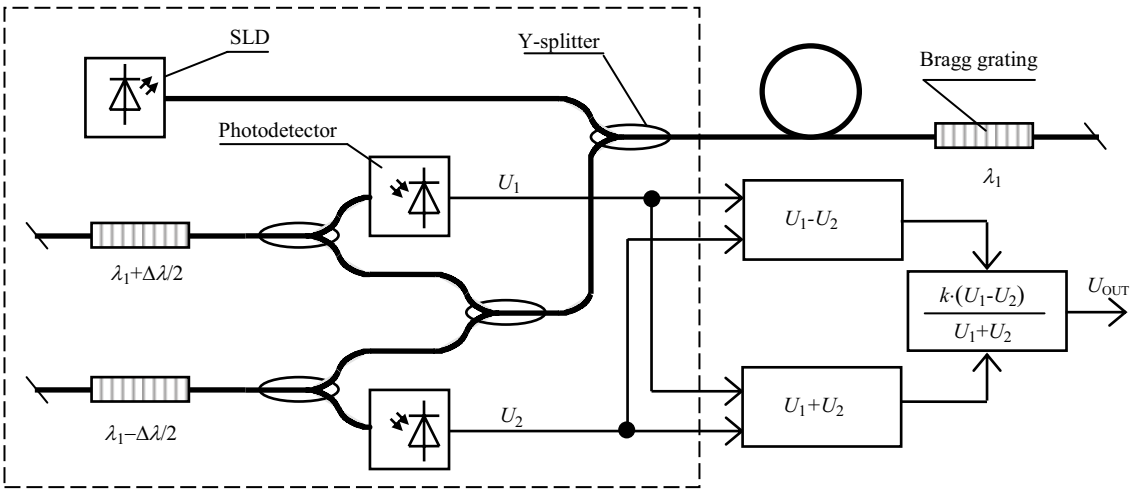

Fig. 1. Signal processing using Bragg gratings as spectral selective elements

The output signal of such a system is described by the equation

$$U_{OUT} = k\frac{U_1 - U_2}{U_1 + U_2} \quad , \tag{1}$$

where k is the transmission factor of the analog divider, U_1 and U_2 are the voltages at photocurrent amplifiers outputs:

$$U_1 = k_1 \int_0^{+\infty} f_1(\lambda) f_S(\lambda) d\lambda \qquad U_2 = k_2 \int_0^{+\infty} f_2(\lambda) f_S(\lambda) d\lambda \tag{2}$$

Here, the values k_1 and k_2 characterize overall transmission coefficient in each channel; $f_1(\lambda)$, $f_2(\lambda)$, and $f_S(\lambda)$ are the reflection spectra of the Bragg grating filters and the Bragg grating sensor, respectively.

The analysis of influence of shift of Bragg gratings spectra on the transmission characteristic of the system was realized by numerical modeling. The analysis has shown that, with an increase in the interval between the maxima of Bragg gratings reflection spectra, the sensitivity of the signal processing system increases, but the nonlinearity of the transmission characteristic also increases. The approach of maxima of reflection spectra of Bragg gratings filters up to 1/3 spectral HWHM allows one to lower nonlinearity

approximately to 4%, which allows one to operate without any special linearization system in many technical applications . However, the sensitivity of a signal processing system is in this case rather small. When a high increase in signal-to-noise ratio is required, the interval between maxima of Bragg gratings filters reflection spectra equal to HWHM may be considered as optimal. In this case, the output signal of the system should be linearized.

Numerical modeling has shown that, for small shifts of Bragg reflection spectrum, the transmission characteristic steepness for the Bragg grating sensor with a spectrum width of 0.3 nm is more than twice larger than the transmission characteristic for the sensor with a spectrum width of 1 nm. At boundaries of deformation range, the transmission characteristic steepness for the sensor with spectrum width 0.3 nm becomes even less than the steepness for the sensor with spectrum width 1 nm. As result, the nonlinearity of the transmission characteristic for the sensor with spectrum width 0.3 nm appears to be greater than for the sensor with spectrum width 1 nm. Thus, there is no need to achieve maximum reduction of the Bragg reflection spectrum width.

To test our system, we made an experiment with registration of plate oscillations after mechanical impact on this plate. A plate of hard aluminum alloy (size 100 x 115 x 2 mm) was used. The Bragg sensor was fixed on the back side of this plate. Excitation of oscillations was made by a shot from a pneumatic pistol to the front side of the plate. One of realizations of processing system signals is shown in Fig. 2. The system allows one to record fast deformation of the plate at the moment of the impact as well as the following damped oscillations.

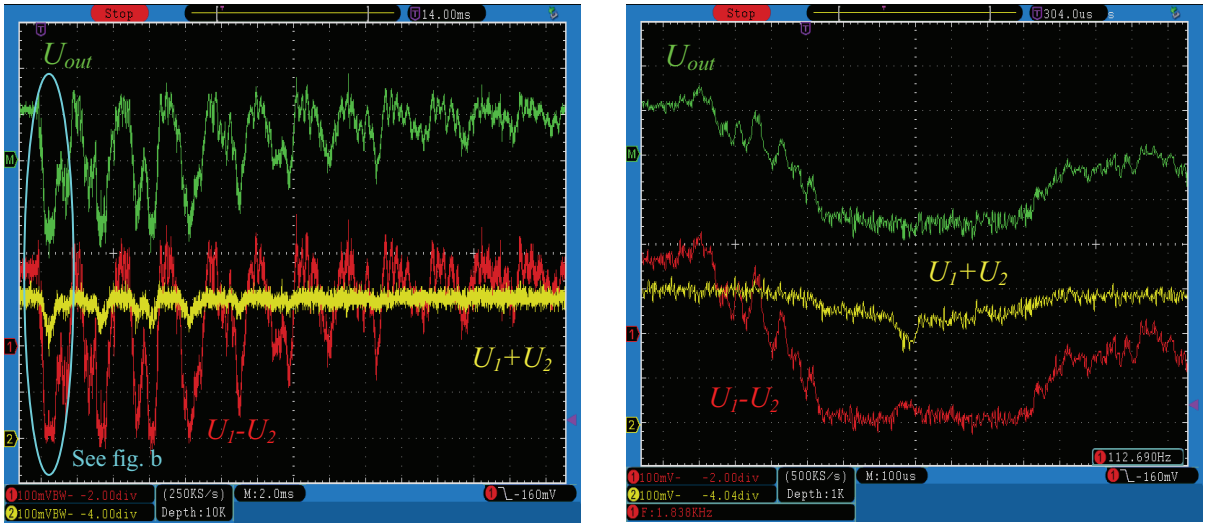

a) b)

Fig. 2. Results of experiment: output, sum and difference signals with resolutions (a) 2 ms/div and (b) 0.1 ms/div

This work was made with support of grant of Russian Foundation for Basic Research, project number 15-48-02317.

References

[1] K. Schroeder, W. Ecke, J. Apitz. Fibre Bragg Grating Sensor System Monitors Operational Load in a Wind Turbine Rotor Blade. Measurement Science and Technology, **17,** 1167-1172 (2006).

[2] V.L. Vesnin, A.A. Chertoriiskii, W. Ecke. Monitoring and Measuring Systems Based on Fiber-Optic Bragg Sensors. Journal of Communications Technology and Electronics, **50,** No 6, 687-693 (2005).

[3] W. Ecke, A.A. Chertoriiski, V.L. Vesnin. A high-speed system for strain and temperature measurements based on fiber Bragg sensors. Instruments and Experimental Techniques, **50,** No 4, 565-571 (2007).

[4] S.A. Babin, S.I. Kablukov, I.S. Shelemba, A.A. Vlasov. An interrogator for a fiber Bragg sensor array based on a tunable erbium fiber laser. Laser Phys, 17, 1340-1344 (2007).

[5] V.L. Vesnin, O.V. Ivanov, A.M. Nizametdinov, A.A. Chertoriyskiy. A fast-response system for a signal processing of fiber optic Bragg sensors on the basis of a differential photodetector. Photon-express, No 6, 238-239 (2015). (in Russian).

Dynamics of Photoinduced Processes in Copper(II) Mixed Halides

Pavel K. Olshin, Alexey V. Povolotskiy, Andrey S. Mereshchenko
Saint-Petersburg State University, 7/9 Universitetskaya nab., St. Petersburg, 199034 Russia
pavel.olshin@spbu.ru

Abstract: Copper(II) tetrahalocomplexes were studied using steady-state absorption spectroscopy and nanosecond transient absorption spectroscopy. Mechanisms of the relaxation of LMCT-excited $[CuCl_4]^{2-}$, $[CuBr_4]^{2-}$ and $[CuClBr_3]^{2-}$ complexes were proposed. Temperature and concentration effects were also investigated.

Recent studies show that copper-based hybrid perovskites ($MA_2CuCl_xBr_{4-x}$, MA – ammonium cation) are very promising as novel hybrid materials because of their optoelectrical activity and they can be used in solar cells and light-emission devices [1]. Conversion of the solar energy occurs as a result of the reversible oxidation of copper(II) ions after being irradiated as a result of ligand to metal charge transfer (LMCT): Cl, Br_pσ → Cu_$d_{x^2-y^2}$ and Cl, Br_pπ → Cu_$d_{x^2-y^2}$. Study of the photoinduced behavior of the complexes will help to understand the possible mechanisms of the charged particles evolution and consequently to find the optimal substances for commercial applications.

The photochemistry of copper(II) halide complexes including $[CuCl_4]^{2-}$, $[CuBr_4]^{2-}$ and $[CuClBr_3]^{2-}$ was studied in this work by means of steady-state absorption spectroscopy and nanosecond transient absorption spectroscopy.

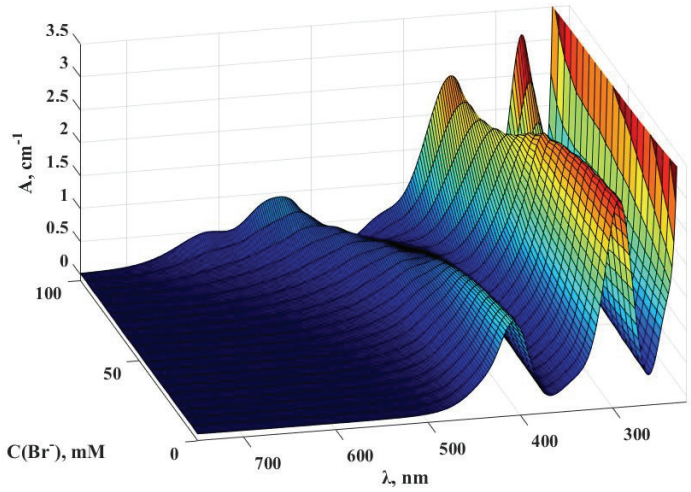

Fig. 1. Spectra of mixed copper(II) mixed halides in acetonitrile; $[CuHal_4]^{2-}$, $Hal^- = Cl^- + Br^-$, $C(Hal^-) = 100$ mM, $C(Cu) = 5$mM.

Optical properties of such compounds strongly depend on the Br/Cl ratio, they possessing absorption in different spectral range (Fig. 1). Synthesis of associated compounds allows easily tuning of the band gap and to find the optimal composition for maximum solar light absorption. It was found previously [2] that the LMCT excited states of the copper(II) chlorocomplexes in acetonitrile can relax through internal conversion mechanism and undergo homolytic or heterolytic dissociation forming radical or ionic products respectively. In case of copper(II) tetrachlorocomplexes the only heterolytic mechanism with formation of ionic products was observed.

The recombination of the ionic products, $[CuHal_3]^-$ and Hal^-, into parent $[CuHal_4]^{2-}$ complexes occurs at the nanosecond time scale though interchange associative mechanism. Recombination bimolecular constants were found to be about $9 \cdot 10^7$ $s^{-1}M^{-1}$ for individual copper(II) tetrachloro- and tetrabromocomplexes. Heating of the copper(II) tetrabromocomplex solutions leads to the photobleaching. This can be accounted for the change in the complex geometry. At the same time, the increase of temperature is likely changing the recombination mechanism.

References

[1] D.Cortecchia, H.A. Dewi, J. Yin, A. Bruno, S. Chen, T.Baikie,P.P. Boix, M. Gratzel, S. Mhaisalkar, C. Soci, and N. Mathews, "Lead-Free MA2CuClxBr4−x Hybrid Perovskites", Inorg. Chem., **55,** 1044-1052, (2016).

[2] A.S. Mereshchenkoa, P.K. Olshin, A.M. Karimov, M.Yu. Skripkin,K.A. Burkov, Y.S. Tveryanovich,A.N. Tarnovsky, "Photochemistry of copper(II) chlorocomplexes in acetonitrile:Trapping the ligand-to-metal charge transfer excited staterelaxations pathways", Chem. Phys. Lett., **615**, 105-110, (2014).

Pico-Femtosecond Image-Tube Instrumentation in Experimental Physics

M.Ya. Schelev
A.M. Prokhorov General Physics Institute, Russian Academy of Sciences,119991 Moscow, 38 Vavilov str.
E-mail: m.schelev@ran.gpi.ru
K.A. Vereshchagin
A.M. Prokhorov General Physics Institute, Russian Academy of Sciences,119991 Moscow, 38 Vavilov str.

Abstract: Analyzed are more than a half-century research experiences in the field of design and application the pico-femtosecond image-tube technologies intended for ultrafast phenomena recording in experimental physics.

Pico-femto-attosecond photoelectronics is the recent trend of technical physics aimed at creation and application of methods and facilities of electron-optical images recording of the fast-proceeding processes (FPP), both of natural and artificial origins.

In the late forties of the last century it appeared demanded the photographic recording of serial phases of images at explosion of the atomic bomb; in the mid-sixties it was required to consider a spatially-temporal picture of a ruby laser radiation in the Q-switched mode. These and similar to them challenges initiated researches on creation and application of methods and tools of pico-femto-attosecond photoelectronics for studying of FPP in the experimental physics. It was the beginning of electron-optical chronography which allowed record FPP with the nano-pico-femtosecond temporal resolution (10^{-9} - 10^{-14} sec).

Photocathodes for transformation of an optical signal to its photo-electric analog are primary detectors in the modern oscillography and are everywhere used in measuring and diagnostic practice. Fast photo diodes and photomultipliers in aggregate provide generation of photo-electric impulses with minimum duration of tens picoseconds (on half-width) at gain factor of an electronic stream up to 10^6 - 10^8. The best stroboscopic oscillographs have a transmission band to several tens GHz now. All this allows measure an intensity temporal profile of weakly glowing the single-pass and repeating fast-proceeding processes in the wide spectral range, determined by sensitivity of photocathodes, with the temporal resolution up to tens of picoseconds. However, fundamental restriction of oscillographic recording methods of FPP is their single-channel nature, i.e. lack of space information on the studied process. Indeed, only the time profile of integral intensity giving only one counting in unit of the recorded time is measured.

Still in the early thirties of the last century the first-ever electron-optical converter (EOC) [1] was created. In EOC the optical pattern was projected on a photocathode, transformed to photoelectronic analog and in the accelerating electric field was plane-parallel transferred to the cathodoluminescent screen plane where the inverse transformation of the photoelectronic image in the visible one was made. Introduction in EOC with electrostatic focusing of the deflecting plates, similar to that are used in an oscillograph led to creation of the time-analyzing EOC. The first time-analyzing EOC capable to record images of separate FPP phases due to switching of the photoelectronic bunches carrying information on the optical pattern were successfully applied in a nuclear physics and a plasma physics. With the help of the time-analyzing EOC simultaneous recording of spatial FPP-pictures with a capacity up to 10^3-10^8 spatially resolved elements with sizes of 10-30 microns in the spectral range from weak roentgen (unit of nanometers) up to near IR (1600 nanometers) and to 3 microns in the mode of a multiquantum photoeffect became possible [2]. With that, quantum effectiveness of some photoemitters in certain spectral areas can reach tens of percent. Use of image intensifiers (cascade EOC, image amplifier based on microchannel plates, modern CCD matrixes, etc.) provide reliable registering of individual photoelectrons in each space element of the recorded image. In the one-photon photoeffect mode the dynamic range of recording on intensity reaches values of 10^3-10^6 and eventually is limited by electrons Coulomb repulsion in the bunch carrying the photoelectronic image.

In Fig.1a the typical design of time-analyzing EOC with the electrostatic focusing lens and one couple of deflecting plates is schematically presented [3,4]. An optical pattern, limited by a slit, projected on a photocathode «1», turned into the photoelectronic analog which accelerates in an interspace between a photocathode and a fine-grain grid «2», gets to the area of the focusing field operated by an electrode «3», passes in an aperture of the accelerating anode cylinder «4» and is undergone to the linear scanning in the deflection system «5» driven by the pulses generator «6». On the image target «7» the spatial image of initial photoelectronic analog scanned in time is registered.

The major parameter of the time-analyzing EOC when recording FPP-images in visible spectral range is its temporal resolution, a theoretical limit to which ~ 10 fs (10^{-14} s). In practice the whole complex of the reasons limiting achievement of the extreme temporal resolution was revealed [2]. Among them both a problem of minimum duration of the photoemissions act for formed in EOC low-impedance oxygen-silver-caesium

a b

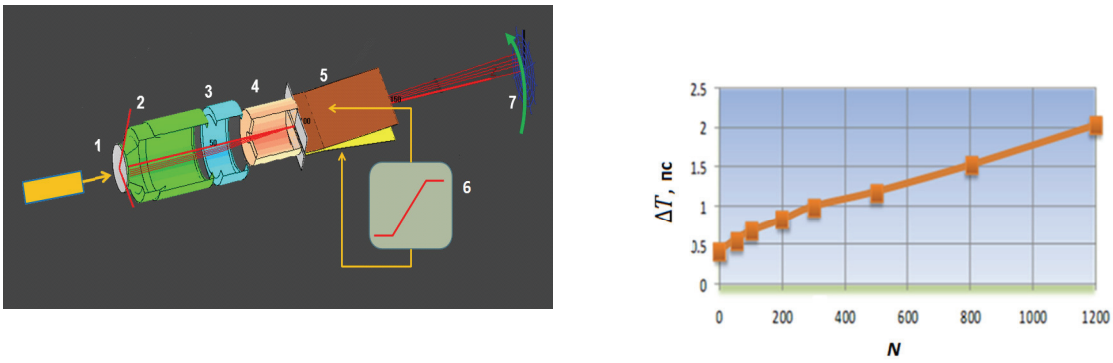

Fig.1. a) Structure of electrodes of time-analyzing EOC with the linear scanning of slit-hole images: 1 – photocathode, 2 – fine-grain accelerating grid, 3 – focusing electrode, 4 – anode, 5 – deflection system, 6 - scanning pulses generator, 7 – timage target (a luminescent screen or a CCD chamber).
b) Dependence of the supreme temporal resolution ΔT on quantity of interacting electrons N in a bunch for EOC with electrostatic focusing.

photocathodes (Ag - About - Cs), and subsequent "swelling" of the photoelectronic bunch generated by a photocathode at its driving to the screen, taking into account the numerous higher aberrations brought by the focusing electronic lens and a deflection system.

In Fig.1b the dependence of the supreme temporal resolution (without the dynamic aberrations brought by scanning system) ΔT on quantity of interacting electrons N in a bunch is presented for EOC with electrostatic focusing [4]. Calculations were carried out at electric field strength on photocathode E_0 = 3kv/mm, anode potential U_a = 12 kV and half-width of initial power distribution of photoelectrons Δ ε = 0.25 eV (HWHM). Apparently, existence in the electron bunch carrying the photoelectronic image of a photocathode only 300 interacting electrons gives, in conditions of numerical experiment, more than to double falling of the supreme temporal resolution: from ~ 400 fs to 1 ps.

The electron-optical cameras, created by us, are successfully used by the Russian and foreign researchers in the various field of science and technique, including: physics of lasers, laser plasma and laser thermonuclear fusion, spectroscopy, non-linear, integrated and fiber optics, photobiology, medicine, femtochemistry, synthesis of new materials, physics of semiconductors, space researches, diagnostics of synchrotron radiation, etc.

[1] Holst G., De Boer J.H., Teves M.C. et al. «An apparatus for the transmission of light of long wavelength into light of short wavelength». - British Patent 326200 D.R.P. 535208 (1928). Physica,**1**, 295—305 (1934).

[2] E.K. Zavoisky, S.D. Fanchenko. «Image-converter high-speed photography with 10^{-9} – 10^{-14} s time resolution». – Appl. Opt, **4**, №9, 1155-1166 (1965).

[3] V.P. Degtyareva, Yu. V. Kulikov, M.A. Monastyrski, et al. «The new streak image tube PIF-01». – In Proc. 16-th Intern. Congr. on High-Speed Photography and Photonics, Proc. SPIE, Vol. 491, p.p. 239-242, Strasbourg, France (1984).

[4] D.E. Greenfield, M.A. Monastyrskiy, V.A. Tarasov. «Software demonstrations». - Abstracts book, "CPO-7" Int. Conf., p.23, Cambridge, UK (2006).

New generation of streak tubes producing by VNIIA

P.I. Konovalov, A.Yu. Sokolov, R.I. Nurtdinov, M.P. Vikulin, I.G. Pryanishnikov, A.S. Dolotov

Dukhov Research Institute of Automatics (VNIIA), 22, ul. Sushchevskaya, Moscow 127055, Russia

Abstract: In 2015, VNIIA Research & Production Center for Pulsed Technique implemented a new technological platform for manufacturing of vacuum electronic devices that made it possible to produce streak tubes with improved key parameters. The platform is based on the finish processing of tubes using transfer technology, which involves producing a photocathode within an individual vacuum volume followed by its transfer to the case and sealing. Using the transfer technology allowed to avoid direct contact of alkali metals with the streak tube internal parts during photocathode formation, which in turn, together with the introduction of ceramic-and-metal envelope allowed a significant increase of dielectric strength of insulators. As the result, the new generation of streak tubes operates at high electric field strength modes and allows to obtain the maximum time resolution up to 0.7 ps. Transition to ceramic-and-metal envelope increased the accuracy and reproducibility of its dimension; using special fitment made a high-precision assembly of streak tubes possible. Thanks to introduction of a number of special technologies for photocathode substrate preparation its effective resistance was reduced and its sensitivity was increased manifold. The introduction of technological improvements mentioned above allowed to create a new generation of streak tubes with improved capabilities. High-precision assembly and increase of the field strength made it possible to increase the streak tube resolution from 20 lines/mm to 30 lines/mm. Increase of the field strength, reduction of the dark current noise, lower photocathode resistance and increase its sensitivity led to an increase dynamic range of streak tube by an order of magnitude: from 1,300 to 10,000. The new generation streak tubes have smaller weight and dimensions and outperform their predecessors in almost all features, including time resolution, dynamic range and life time.

Lasers and streak-cameras at physics of accelerators

Oleg I. Meshkov
Budker Institute of Nuclear Physics, Novosibirsk, Russia

Ultra-relativistic beams of particles in modern linear and cyclic accelerators have a typical spatial longitudinal dimension between tenths of a millimeter up to tens of millimeters. This value needs of a constant monitoring. It means a necessity of measurement of time intervals lasting from ten to tens of picoseconds with an accuracy of a few percent. In recent years, along with the application for these purpose streak cameras, the methods of particle beam diagnostic based on the application of laser radiation are widely used. Lasers are applied for precise measurements of geometric dimensions and the energy of the beams as well as for generation of intense X-ray fluxes. Laser scattering is able to vary an energy spread of the particles in a beam. The report reviews the application of lasers, streak cameras and optical dissectors for measurements and operations of particle beams in modern electron and positron accelerators.

Two photon processes for a fast timing in nuclear instrumentation.

Mikhail Korjik[1], Oleg Bugnavov[2], Andrei Fedorov[1], Vitaly Mechinsky[1], Sergei Tichomirov[2], Gintautas Tamulaitis[3], Etiennette Auffray[4], Marco Lucchini[4]

1- Institutte for Nuclear Problems of Belarus State University, Minsk, Belarus
2-B.I.Stepanov Inst. Of Physics, Minsk , Belarus
3-Vilnius University, Vilnius , Lithuania
4-CERN, Geneva, Switzerland

Abstract

Here we report first results of the study by two photon absorption methods of the ultra-fast phenomena in inorganic scintillation materials with the purpose to develop new detecting techniques of ionizing radiation.

The upcoming experiments in high-energy physics require the time resolution of scintillation detectors better than 10-20 ps. This is not feasible using the conventional scintillation detectors with the time response limited by the time of carrier relaxation and transfer to the radiative recombination centers in the scintillator material.

In this study, we investigate the feasibility of using the phenomena occurring in parallel with the carrier relaxation within the very first picoseconds after the ionization starts. One of the phenomena is the elastic polarization due to the local lattice distortion caused by the displacements of electrons and holes generated by the ionization. This local distortion in the lattice results in redistribution of the density of states (DOS) of electron in the conduction band in close vicinity of the hole. The key feature of the elastic polarization is its short response time, which makes it prospective for using as an optically detectable time mark. Nonlinear optical absorption of femtosecond light pulses at appropriate wavelength is considered to be a tool to form the mark.

The effect of elastic polarization should be observed in many crystalline compounds. According to our estimations, the strongest effect should be observed in compounds with the bottom of the conduction band formed by ***n*d** orbitals of the lattice cations. According to the crystal field theory, these orbitals are most sensitive to distortions of the crystal field in the vicinity of emitting centers. Thus, the crystals with lattice cations having strong contribution of **d** orbitals in conduction band (tungstates, molibdates, rare-earth and yttrium garnets, perovskites, oxy-orthosilicates, etc.) might be good candidates for using them as timing tools.

Our study was aimed at searching for inorganic crystalline media exhibiting good scintillation properties as well as strong non-linear absorption of ultra-short laser pulses. Accordingly, we selected three scintillation crystals: self-activated lead tungstate $PbWO_4$ and mixed $Gd_3(Ga_{0.5}\text{-}Al_{0.5})_5O_{12}$:Ce and yttrium $Y_3Al_5O_{12}$:Ce garnets. Lead tungstate is currently the most extensively used scintillation material in high energy physics experiments [1], while the recently developed mixed garnet crystals showed fast response and high light yield up to 56000 ph/MeV [2]. YAG:Ce is also fast and bright scintillation material exhibiting one of the highest radiation

hardness among the scintillators currently in use under both gamma and high energy proton irradiation [3]. Recently, we confirmed the influence of ionization at 122 keV on the two photon absorption of femtosecond laser pulses in $PbWO_4$ crystals [4]. The observed effect encouraged our further study in this direction to develop a novel detecting technique exploiting the interaction of short laser pulses with crystalline media excited by ionizing radiation. The results of this study are presented in the current paper. In addition to pure scintillation materials synthetic diamond was probed with two-photon absorption.

One-photon absorption is extensively used to monitor different effects in ionizing radiation detectors. For instance, nanosecond laser pulses are used to monitor radiation damage effects in PWO crystals [5]. In fact, this technique enables monitoring slow change in the detector material properties, particularly accumulation of the color centers under ionizing radiation.

One-photon absorption is not convenient to explore changes in the DOS due to strong absorption of single photons via electronic transitions between valence and conduction bands. This is due to the origin of the bands of the majority of inorganic wide band gap compounds: p electronic states form the top of valence band, whereas d and f states of metal ions dominate in forming the bottom of the conduction band. Dipole-allowed p-d transitions result in the absorption coefficient for the interband transitions at the order of $10^5 cm^{-1}$.

The selection rules for two-photon absorption are different [6]: p-d transitions become forbidden and their rate falls by orders of magnitude. Consequently, the photons absorbed via two-photon absorption propagate relatively long distances in the crystal.

Two-photon absorption can involve photons of the same frequency generated by the same laser or simultaneously available photons of different frequencies [7]. The two-photon absorption involving one pump and one probe photon is a convenient tool for studying both time and spectral parameters of the interband absorption. Recently, the pump-probe technique was exploited to study $PbWO_4$ crystals [8]. The pump-induced changes in material properties resulting in modified probe absorption in the sample volume where the pump and probe beams spatially overlap have been recorded.

Literature

1. A. Annenkov, M. Korzhik, P. Lecoq. Lead tungstate scintillation material. Nucl. Instr. and Meth. in Phys. Res. A, 490 (2002) 30-50
2. K. Kamada, T. Yanagida, T. Endo, K. Tsutumi, Y. Usuki, M. Nikl, et al., J. Cryst.Growth 352 (2012) 88–90.
3. [3] K.-T. Brinkman, A. Borisevich, et.al., Radiation Damage and Recovery of Medium Heavy and Light Inorganic Crystalline, Glass and Glass Ceramic Materials after Irradiation With 150MeV Protons and 1.2MeV Gamma-Rays, IEEE NSS-MIC Conference record, 2014
4. Auffray, O. Buganov, M. Korjik, A. Fedorov, S. Nargelas, G. Tamulaitis, S. Tikhomirov, A. Vaitkevicius, Application of two-photon absorption in PWO scintillator for fast timing of interaction with ionizing radiation, Nuclear Instruments and Methods in Physics Research Section A, In Press, Available online 16 September 2015.
5. L. Zhang, A Diode-Pumped Solid State Blue Laser for Monitoring the CMS Lead Tungstate Crystal Calorimeter at the LHC, J. Phys. Conf. Ser., Vol.404 (2012), 012042.
6. N.B.Delone, Interaction of laser radiation with body:Lectures. Moscow, Nauka, 1981, P.280, ISBN 5-02-014056-2 (in Russian).
7. *J.–C. Diels and W. Rudolph,* Ultrashort Laser Pulse Phenomena, Elsevier, 2006, P.647. ISBN:10: 0-12-215493-2
8. E. Auffray, O.Buganov et al., New detecting techniques for future calorimetry, Lournal of Physics: Conf. Series 587(2015) 012056.

Oral contribution to ICONO/LAT 2016 Conference, Minsk 2016

Title:

Andor Technology: advanced and versatile camera technology for nanosecond gated imaging and spectroscopy

Authors:

Thorsten Pieper, LOT-QuantumDesign GmbH, Darmstadt, Germany
Yuri Zheleznov, Moscow, Russia

Abstract:

Scientific imaging in physics applications either requires a high sensitivity, high spatial or high temporal resolution. From Andor Technology there are cameras for each of these tasks. With special emphasize on the observation of fast processes we try to 'illuminate' the variety of available imaging cameras and simplify the choice. A clear distinction between intensified and non-intensified, gated and non-gated cameras is made. Starting from the level of CCD we compare the concept of ICCD cameras and introduce Andor Technology's new intensified sCMOS camera. Improvements in pixel resolution, read noise and frame rate are discussed.

A new method of electron scrubbing of microchannel plates

P.I. Konovalov, A.S. Dolotov, R.I. Nurtdinov, M.P. Vikulin

Dukhov Research Institute of Automatics (VNIIA), 22, ul. Sushchevskaya, Moscow 127055, Russia

Abstract: Using ion-barrier film significantly reduces the technical characteristics of photoelectric devices, so the task of its exception from the device is extremely important. One of the possible ways to eliminate ion-barrier film is the development of new methods of outgassing microchannel plates (MCPs) to reduce the residual gas emission and intensity of electron-stimulated desorption to a level at which the lack of ion-barrier film will not affect the lifetime of the device. It was proposed a new method of electron scrubbing of microchannel plates, which periodically changes the direction of the flow of electrons inside the MCP channels with simultaneous change of voltage polarity on the MCP. It is shown that the residual gas emission intensity in the channels after bilateral electron scrubbing of microchannel plates is much less than after unilateral. In addition, the gain of MCP after unilateral and bilateral electron scrubbing of microchannel plates is almost identical. This leads to the assumption that bilateral electron scrubbing of MCP can solve the problem of using the ion-barrier films in photoelectric devices.

Ultrafast Deactivation of Excitation Energy in Rutin and Quercetin via Electron and Proton Transfers

S.L. Bondarev, S.A. Tikhomirov, V.N. Knyukshto, O.V. Buganov, T.F. Raichyonok, A.D. Shirokanov
B.I. Stepanov Institute of Physics, National Academy of Sciences of Belarus,220072 Minsk, Nezavisimosti av. 70, Belarus
e-mail: stan.bond.1944@gmail.com; fax: + 375 17 284-08-79

Abstract: Using femtosecond spectroscopy and steady-state luminescence methods, the mechanisms of very fast non-radiative deactivation ($k_{nr} \sim 5\times10^{11}$ c^{-1}) of the electronic excitation energy at room temperature in organic and buffer solutions of well-known natural antioxidants rutin and quercetin have been studied.

Quercetin (QU) and rutin (RU) belong to the flavonoids (FV). They are a large class of polyphenolic natural pigments found in all land-based green plants [1]. The molecular structure shown on Fig. 1, contains two benzene rings (A and B) linked through a heterocyclic pyran ring C (with a double bond) and disaccharide rutinose (RU) or H (QU) as substitutes in 3-position (R). Among a large number of FV, RU and QU are remarkable for their expressive properties to antagonize the increasing in capillary fragility, to reduce high blood pressure, to serve as antioxidants, *etc*.

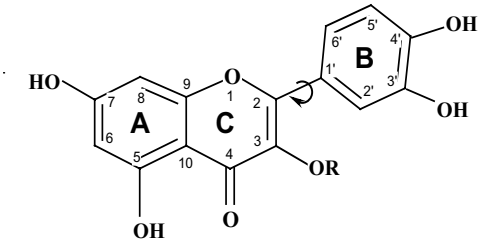

Fig. 1. Chemical structures of rutin and quercetin in methanol

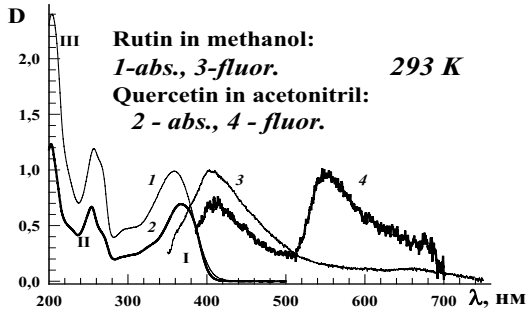

Fig.2. Absorption, fluorescence spectra of RU and QU in acetonitrile at 293 *K*

RU and QU are biosynthesized from the amino acid phenylalanine under enzymatic control activated by UV solar radiation [2,3]. The main part of solar radiation in the region 320-400 nm (UV-A) reaches the Earth′s surface participating in damaging photochemical reactions in plants and human skin. It is believed that FV play an important role in the protection of UV-sensitive molecules in living tissues owing to their strong absorption in UV-A region. Accepting high intensity sunny light, the FV has a possibility to save their primary biochemical and spectral properties. Knowing this natural quality of such biological active pigments, we solved to investigate the mechanisms of the effective deactivation processes of electronic excitation energy for rutin and quercetin in organic and buffer solutions at room temperature and 77 K.

Absorption spectra of RU and QU in methanol consist of three vibronic bands with maxima at 357 nm (band I), 257 nm (II) and 205 nm (III). The weak fluorescence spectrum for RU in methanol with a maximum at 415 nm under λ_{exc} = 340 nm was observed at 293 K (Fig. 2). The measured fluorescence quantum yield Φ_{fl} was equal to $2.0\text{x}10^{-4}$. For QU in acetonitrile the value of Φ_{fl} is approximately the same. The radiative and non-radiative decay rates of RU are $7.5\text{x}10^{7}$ s^{-1} and $3.7\text{x}10^{11}$ s^{-1}, respectively.

Large increase of rutin's fluorescence intensity is observed at 77 K. The emission spectrum of RU in ethanol consists of two bands (Fig. 3): an intensive short-wavelength band at 415 nm and a weak band at 540 nm. The former emission band belongs to the normal Stokes' shift fluorescence and the second one belongs to the phosphorescence. In the case of QU, there are also 2 emission bands at 293 K and 77 K which are characterized as a fluorescence of solvated molecules of QU at 420 nm and photo-tautomer with intramolecular proton transfer in excited state at 545 nm [4].

The femtosecond measurements of RU and QU solutions at room temperature allowed revealing the transient absorption spectra at $\lambda_{max} \sim 460$ nm in all used solvents (Fig. 4). The deactivation kinetics in all studied solvents are exponential, and the measured lifetimes are located in the range 10,0 – 20,0 ps. As seen from Fig. 4, the spectra reach the maximum within 1,0 ps and organic vanish absolutely through 100,0 ps. The triplet-triplet absorption wasn't revealed in all spectral region.

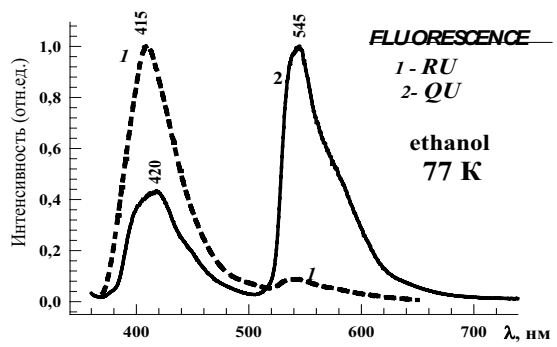

Fig. 3. Luminescence spectra of RU (1) and QU (2) in ethanol at 77 K

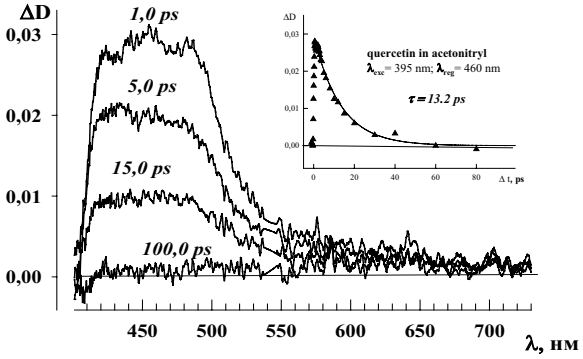

Fig. 4. Transient absorption spectra and kinetics of QU in acetonitrile at 293K

The femtosecond measurements of RU and QU organic solutions at room temperature allowed revealing the transient absorption spectra at λ_{max} ~ 460 nm in all used solvents (Fig. 4). The deactivation kinetics in all studied solvents are exponential, and the measured lifetimes are located in the range 10,0 – 20,0 ps. As seen from Fig. 4, the spectra reach the maximum within 1,0 ps and vanish absolutely through 100,0 ps. The triplet-triplet absorption wasn't revealed in all studied spectral region.

From these data along with very low fluorescence quantum yield at room temperature we can propose the mechanisms of very effective non-emission deactivation in RU and QU. The differences in structural and spectral properties for these two flavonoids have determined the differences in their non-emission channels of electronic excitation energy deactivation. The first difference is in large spectral shift of the low excited state in QU as compare with RU: 24 100 cm^{-1} (415 nm) for RU and 18 500 cm^{-1} (540 nm) for QU. However, the form and kinetic of transient absorption spectra at room temperature for RU and QU are practically the same. This fact means that part of RU and QU molecules deactivate the same way. This way is determined by the solvates of RU and QU molecules which are organized in the ground state. The another non-solvated part of RU molecules must possess a very small probability of direct internal conversion due to very large energy gap ΔE $(S_1,S_0) \approx 27800$ cm^{-1}. However, it is observed an opposite process of high rising of internal conversion. Our explanation of that unusual behavior is consists in the new transient excited state appearing. That transient state has the charge (electron) transfer (CT) character. The Frank-Condon excited states of RU and QU are characterized by high dipole moments $46{,}6\times10^{-30}$ C m and $52{,}8\times10^{-30}$ C m, respectively. The adiabatic potential energy of this CT state is changed in dependence of the rotation angle of B-ring around 2 – 1′-bond. The strong electron transfer is proposed between B–ring and 4-CO carbonyl group. In the case of QU the formation CT state and localization of the excess electron density at 4-CO carbonyl group promote additionally the intramolecular proton transfer with formation photo-tautomer. Therefore, the main channel of non-emission deactivation of the electronic excitation energy in RU and QU is the S_1~~>S_0 internal conversion induced by the CT state.

[1] J.A. Rothwell, A.J. Day and M.R.A. Morgan, «Experimental determination of octanol-water partition coefficients of quercetin and related flavonoids», J. Agric. Food Chem. 53 4355 – 4360 (2005).
[2] J.B. Harborne and C.A. Williams,«Advances in flavonoid research since 1992», Phytochemistry, 55 481 – 504 (2000).
[3] A. Gaberscik, M. Voncina, T. Trost and M. Germ, «Growth and production of buckwheat (Fagopyrum esculentum) treated with reduced, ambient, and enhanced UV-B radiation», J. Photochem. Photobiol. B: Biol. 66 30 – 36 (2002b).
[4] E. Falkovskaia, P.K. Sengupta and M. Kasha, «Photophysical induction of dual fluorescence of quercetin and related hydroxyflavones upon intermolecular H-bonding to solvent matrix», Chem. Phys. Lett. 297 109 – 116 (1998).

X-ray Diffractometry with Synchrotron Radiation for Exploration of Fast Processes in Solids with Nanosecond Time Resolution

B.P.Tolochko, O.V.Evdokov
Institute of Solid State Chemistry and Mechanochemistry Siberian Branch of Russian Academy of Sciences, 630128 Novosibirsk, 18 Kutateladze str.
e-mail address: B.P.Tolochko@inp.nsk.su
K.A.Ten, I.A.Rubtsov, E.R.Pruuel, A.O.Kashkarov
Lavrentiev Institute for Hydrodynamics Siberian Branch of Russian Academy of Sciences, 630090 Novosibirsk, 5 Lavrantev str.
A.S.Arakcheev, V.M.Aulchenko , A.V. Burdakov, A.D. Chernyakin, G.N.Kulipanov, A.A.Kasatov , A.V. Kosov , P.A. Piminov, S.V. Polosatkin, V.A. Popov, L.I. Shekhtman , A.A. Shoshin, D.I.Skovorodin, A.A. Vasilyev , L.N. Vyacheslavov, V.V. Zhulanov, K.V.Zolotarev
Budker Institute of nuclear Physics Siberian Branch of Russian Academy of Sciences, 630090 Novosibirsk, 11 Lavrantev str.

Abstract: The report is reviews the principles of nanosecond X-ray diffractometry with using synchrotron radiation and requirements to object, equipment and detectors. Investigation of pulsed laser radiation and shock waves impact on the substance was made.

The technique of X-ray diffraction with time resolution has shown tremendous progress recent years. This is due to the development of the accelerator technology, methods of generation of synchrotron radiation (SR), and fast X-ray detectors. The report reviews the main principles of time-resolved X-ray diffractometry and requirements to the object, equipment and detectors. Considered are the basic parameters of the diffraction installations at BINP, SLAC, and EuXFEL.

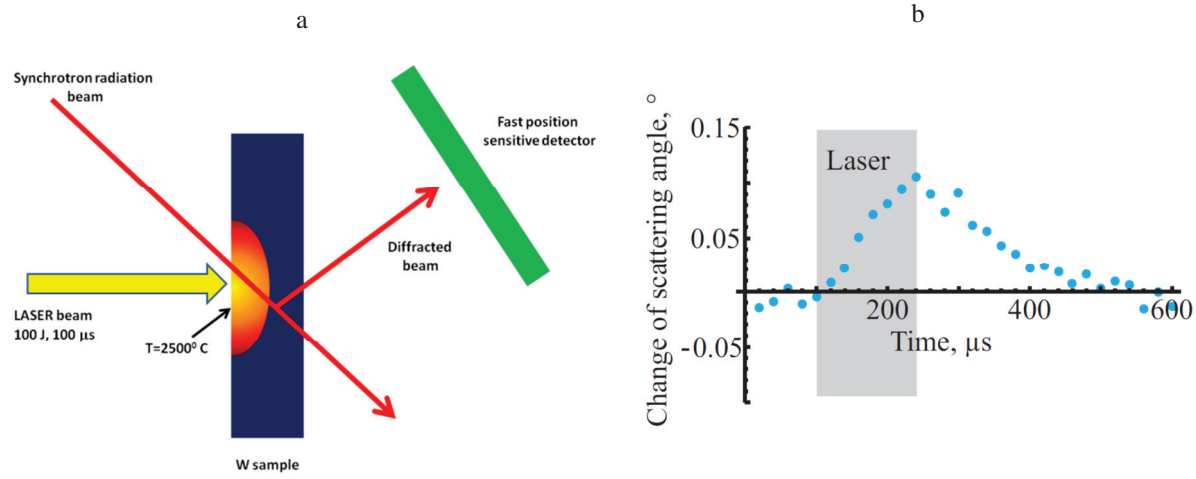

Fig. 1. a) Scheme of fast 100 J laser heating experiment. The laser beam heats the surface of the sample up to 2500 C, which gives rise stresses around the heating zone. Synchrotron radiation allows to measure the dynamics of the stress developing and the dynamics of their relaxation.
b) The time dependencies of the change of the X-ray diffraction angle during 1 J laser heating caused by stress. The grey background marks the time interval of the laser heating.

To obtain the best experimental parameters it is necessary to minimize the duration of the SR flash and the divergence of the primary beam, as well as increasing its intensity and monochromaticity. Unfortunately, currently it is impossible to improve all the parameters simultaneously, so the experimenters have to compromise. For example, they increase the flux of photons at the expense of deterioration of the monochromaticity (BINP and APS/ANL) and carry out experiments in the "pink" spectrum. Or they increase the exposure time at the expense of summation of photons from a few bunches. This mode was applied to investigation into the dynamics of nucleation and growth of nanodiamonds in a shock-wave impact on hydrocarbons. Possible options of development of time-resolved X-ray diffractometry installations at BINP are considered.

Now we are preparing an experiment to study the behavior of the crystal lattice of the material of the fusion reactor first wall during a plasma discharge on the diverter. A fast one-coordinate X-ray detector was developed

for this experiment. The detector enables fast recording of 100 diffraction frames with an exposure time of 73 ps and a periodicity of 100 ns. Thus, we can record X-ray "movies" with high time resolution, which store information about the dynamics of plasma interaction with the structure of the crystal surface in a plasma discharge (100 μs in the ITER).

To solve this problem we are developing an installation to work on beams of synchrotron radiation of VEPP-4 (BINP SB RAS). The installation will enable obtaining information about what is happening to the crystal lattice when the plasma of the ITER reactor interacts with the wall for a short period of time. The plasma discharge parameters in the ITER are as follows: an energy of 100 J for 100 μs on an area of 1 mm2. We conducted first successful test experiments, having recorded changes in the crystal lattice of W, using a laser with a power of 1 J and a pulse width of 100 μs. Now diffraction patterns with a time resolution of 73 ps can be recorded.

Installation scheme is shown in Figure 1-a. Specificity of the experiment is that 100 J laser heats a very thin surface layer, and as result at the heat front the internal stresses appears. As heat front move into the sample and the stress distribution in the sample is changing. A narrow beam of synchrotron radiation with an energy of 80 keV allows to probe the region of interest of the sample and obtain information about the distribution of stresses during laser heating of the sample. Experimental results are presented in Figure 1-b

The same method will be used for investigation the behavior of the crystal lattice of space materials under the impact of shock waves and meteorites, flying with speeds of up to 11 km/sec. For this experiment, a gun launching small pellets with such speeds has been designed.

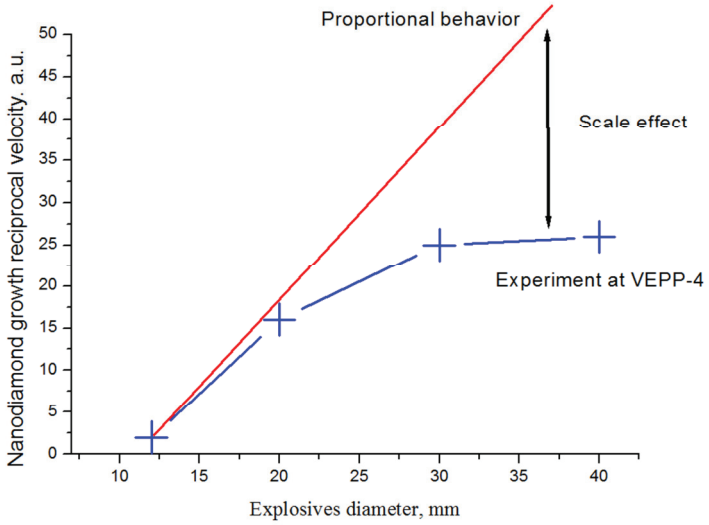

Fig. 2. The dynamics (velocity) of nanodiamonds mass during detonation (+). The curve is a non-trivial, non-linear dependence versus the mass of explosives (explosive diameter).

Our group has more than 15 years investigate the dynamics of nanodiamonds formation during detonation and shock wave effects. In recent experiments obtained reliable experimental data showing the growth dynamics of nanodiamonds during detonation of TNT. This is a unique result, since similar experiments conducted in Advance Photon Source (US, Argonne National Laboratory) have not detected an increase the size of the diamond. The data obtained allow to plan experiments in which the authors hope to grow diamond with micron sizes.

In the study of the dynamics of formation of nanodiamonds during detonation was received scale effect - a non-trivial, non-linear dependence of the all diamond mass in the reaction zone versus the mass of explosives (explosive diameter, Fig.2.).